ESAIM: Control, Optimisation and Calculus of Variations May 1998, Vol. 3, 163–212
URL: http://www.emath.fr/cocv/

GEOMETRICAL ASPECTS OF EXACT BOUNDARY CONTROLLABILITY FOR THE WAVE EQUATION – A NUMERICAL STUDY

M. ASCH AND G. LEBEAU

Abstract. This essentially numerical study, sets out to investigate various geometrical properties of exact boundary controllability of the wave equation when the control is applied on a part of the boundary. Relationships between the geometry of the domain, the geometry of the controlled boundary, the time needed to control and the energy of the control are dealt with. A new norm of the control and an energetic cost factor are introduced. These quantities enable a detailed appraisal of the numerical solutions obtained and the detection of trapped rays.

Contents

Mark Asch, Laboratoire d'Analyse Numérique, Université Paris XI, 91405 Orsay, France. E-mail: Mark.Asch@math.u-psud.fr.

Gilles Lebeau, CMAT, École Polytechnique, 91128 Palaiseau, France. E-mail: Gilles.Lebeau@math.polytechnique.fr.

Received by the journal June 12, 1997. Revised October 1, 1997 and March 2, 1998. Accepted for publication March 31, 1998.

1. Introduction

The motivation for this paper comes from three sources:

- the Hilbert Uniqueness Method (HUM) formulated by J.-L. Lions – see [8];
- the numerical application of the above method to exact boundary control of the wave equation by R. Glowinski *et al.* – see [6, 7];
- the geometrical results of Bardos, Lebeau and Rauch [4] which enabled the proof of sharp sufficient conditions for control of the wave equation from the boundary.

The geometrical result concerning the exact boundary controllability of the wave equation as obtained by [4], states that one must control on a set large enough to encounter every ray of geometric optics. However, this is not very intuitive, especially when the geometry of the controlled domain becomes complicated and when the control is applied on a part of the boundary only. This numerical study will try to illustrate and elucidate various aspects of this theoretical result.

We remark that apart from the numerical studies of [6, 7] cited above, [5] have also performed a numerical investigation of the controllability of a non-linear wave equation (in one space dimension) with the control located in a small neighborhood of the boundary.

In this paper we begin by recalling the main theorems concerning the Hilbert Uniqueness Method of J.-L. Lions [8] and the geometrical theorems of Bardos-Lebeau-Rauch [4]. We then explain the numerical algorithm which closely follows the work of R. Glowinski [6]. After a validation of the code, we use it to study various relations between

- the geometry of the control boundary;
- the time needed to control a given geometrical configuration;

- the oscillatory nature of the data;
- the cost of the control.

We seek in particular a numerical manifestation of the trapped ray phenomenon. Finally we draw some conclusions.

2. The HUM approach to exact boundary controllability

2.1. Formulation of the problem

We consider the wave equation with control on a *part* of the boundary,

$$\begin{cases} \Box u = 0 \quad \text{in } Q = \Omega \times (0,T), \\ u(x,0) = u^0, u_t(x,0) = u^1 \quad \text{in } \Omega, \\ u = \begin{cases} g & \text{on } \Sigma_0 = \Gamma_0 \times (0,T), \\ 0 & \text{on } \Sigma \setminus \Sigma_0 = \Gamma \setminus \Gamma_0 \times (0,T) \end{cases} \end{cases} \tag{2.1}$$

where Ω is a bounded domain of $\mathbb{R}^2$ with boundary Γ, and $\Gamma_0 \subset \Gamma$. In other words, the boundary control is applied on the part Γ_0 of the boundary Γ.

The problem of exact boundary controllability is then: "Given T, u^0, u^1, can we find a control g on Σ_0 such that the solution of (2.1) satisfies

$$u(x,T) = u_t(x,T) = 0 \text{ on } \Omega \text{ ? }"$$

The answer is yes, if

- one takes T sufficiently large, and
- one controls on a set large enough to encounter every ray of geometric optics (see below).

This answer raises numerous questions:

- how does T depend on the geometry of the domain ?
- How does T depend on the spectrum of the initial data ?
- For complicated geometries, what constitutes a set "large enough to encounter every ray of geometric optics" ?

All these questions will be treated in the sequel.

A systematic and constructive method for computing such a control, g, is provided by the *Hilbert uniqueness method* (HUM) of Lions [8].

2.2. Description of the HUM

We now describe briefly the HUM for control of the wave equation from a part of the boundary. Full details can be found in [8].

Let

$$E = H_0^1(\Omega) \times L^2(\Omega), E' = H^{-1}(\Omega) \times L^2(\Omega)$$

and define the operator

$$\Lambda : E \to E'$$

as follows:

1. Take $\mathbf{e} = \{e^0, e^1\} \in E$ and solve from $t = 0$ to $t = T$

$$\begin{aligned} \Box\phi &= 0 \quad \text{in } \Omega \times (0,T), \\ \phi(x,0) = e^0, \phi_t(x,0) &= e^1 \quad \text{in } \Omega, \\ \phi(x,t) &= 0 \quad \text{on } \Gamma \times (0,T) = \Sigma. \end{aligned} \tag{2.2}$$

2. Then solve (backwards) from $t = T$ to $t = 0$

$$\begin{aligned} \Box\psi &= 0 \text{ in } \Omega \times (0,T), \\ \psi(x,T) = 0, \psi_t(x,T) &= 0 \text{ in } \Omega, \\ \psi(x,t) &= \begin{cases} \frac{\partial\phi}{\partial n} & \text{on } \Sigma_0 = \Gamma_0 \times (0,T), \\ 0 & \text{on } \Sigma \setminus \Sigma_0 = \Gamma \setminus \Gamma_0 \times (0,T). \end{cases} \end{aligned} \tag{2.3}$$

3. Finally, define the operator Λ as

$$\Lambda \mathbf{e} = \{\psi_t(0), -\psi(0)\}.$$

We have the original theorem of J.-L. Lions [8]:

THEOREM 2.1 **(J.-L. Lions)**. *Operator Λ is linear and continuous from E onto E'; moreover, if T is sufficiently large ($> T_{min} = 2\|x - x_0\|_{L^\infty(\Omega)}$) and if Γ_0 is of the type*

$$\Gamma(x_0) = \{x \,|x \in \Gamma, (x - x_0) \cdot n_x > 0\}$$

where $x_0 \in \mathbb{R}^2$ is an arbitrary point and n_x is the outward normal to Γ at x, then Λ is an isomorphism *from E onto E'.*

2.3. Application of the HUM to the wave equation

Let us now apply Theorem 2.1 to the control of the wave equation (2.1). Suppose that

$$u^0 \in L^2(\Omega), u^1 \in H^{-1}(\Omega)$$

are given. Then

1. take $\mathbf{f} = \{u^1, -u^0\}$ – *i.e.* we identify u with ψ;
2. solve $\Lambda \mathbf{e} = \mathbf{f}$ to obtain e^0, e^1, the initial data for the ϕ wave equation (2.2);
3. solve the ϕ wave equation (2.2) forwards in time using e^0, e^1 as initial data;
4. calculate the normal derivative of the solution of the ϕ wave equation and set $g = \frac{\partial\phi}{\partial n}|_{\Sigma_0}$;
5. solve the ψ wave equation (2.3) backwards in time using g as the boundary data;
6. finally, set $u = \psi$, then since $\psi(x,T) = 0, \psi_t(x,T) = 0$ was imposed, g (the boundary control) gives the exact boundary controllability with

$$u(x,T) = u_t(x,T) = 0, \forall x \in \Omega.$$

We remark that the operator Λ is symmetric and E-elliptic. These properties imply that $\Lambda \mathbf{e} = \mathbf{f}$ can be solved by a conjugate gradient algorithm.

2.4. Control on a part of the boundary: theoretical aspects

We would like to analyze more precisely what happens in the case of control on a *part* of the boundary. This analysis, which appears in Appendix A, motivates the introduction of the energetic cost vector of Section 5.

3. Sharp sufficient conditions for the control of waves from the boundary

In this section we will present a simplified version of the results in [4]. We repeat here a part of the introduction to this paper:

> Finally, we come to the idea/method that motivates our analysis. Wave equations have solutions that are localized near curves $(t, x(t))$ in space-time. The curves are called rays, and typical rigorous results assert that for any $\varepsilon > 0$ and $T > 0$ there is a solution so that the fraction of the energy located at a distance smaller than ε from the ray is greater than $1 - \varepsilon$ for $0 \leq t \leq T$. [...] it would be foolhardy to try to control a solution from a set on which the energy is negligibly small. Thus controls must be placed so that there is a control on every ray [4, p. 1026].

The following classification of rays can be made according to the nature of their contact with the boundary:

- rays that hit the boundary transversally – they are reflected by the classical laws of geometrical optics and their trace at the boundary is comparable in size to the corresponding wave;
- rays that kiss the boundary at a diffractive point – they leave a very small trace;
- rays that hug the boundary (near tangential incidence with non-diffractive contact) – for these gliding rays the traces are comparable in size to the waves.

This last point constitutes the main estimate of [4]. The lower bound on traces thus obtained in a subset of the region of control, is combined with theorems on the propagation of singularities to derive estimates throughout the domain. In fact it is shown that the trace is appreciable for any ray that in the absence of boundary conditions would leave Ω. Such rays are called *nondiffractive*. Special cases are the gliding and transversely reflected rays. Since the boundary is responsible for confining such rays, it is reasonable to expect that the boundary must do appreciable work.

Once the lower bound (in the energy $e = \int_\Omega u_t^2 + |\nabla_x u|^2 + u^2\, dx$),

$$\|u\|^2_{H^1(]0,T[\times\omega)} \geq ce$$

for example, has been obtained, it can be used via a suitable identification of dual spaces to show the strong ellipticity of the map Λ of the HUM. To compute the control we can then use a conjugate gradient method as shown in the next section.

Many interesting examples of control domain geometry (disconnected minimal regions for control on the disk, bowling ball and dogbone) are given in [4] and are compared with results obtainable by multiplier techniques. We appreciate immediately the advantage of the geometrical approach when examining these cases. In fact our numerical study will be based on the intuitions obtained from these very examples.

We can now express the theorem of Lions in its geometrical form:

Theorem 3.1 **(BLR)**. *If all the generalized geodesics of length T meet the control boundary, Γ_0, at a non-diffractive point then for any u^0, u^1 in*

$L^2(\Omega) \times H^{-1}(\Omega)$ one can find a control $g \in L^2(\Gamma_0 \times (0,T))$ which drives the system (2.1) from u^0, u^1 at time zero, to rest at time T.

4. A numerical algorithm based on the HUM

As we will now show, the constructive nature of the HUM together with the favorable properties of the operator Λ, enables us to formulate a numerical algorithm based on the use of a conjugate gradient method with the HUM at its core. This will be presented in three steps:

1. presentation of a general conjugate gradient algorithm (Algorithm CG-0);
2. application of algorithm CG-0 to the boundary controllability problem for the wave equation based on the HUM (Algorithm CG-HUM);
3. discretization of algorithm CG-HUM using a mutltigrid technique (Algorithm CG-h);

4.1. The conjugate gradient solution

We can rewrite problem $\Lambda \mathbf{e} = \mathbf{f}$, taking $\mathbf{f} = \{u^1, -u^0\}$, in the following variational form:

$$\text{Find } \mathbf{e} \in E \text{ such that } \langle \Lambda \mathbf{e}, \check{\mathbf{e}} \rangle = \langle \{u^1, -u^0\}, \check{\mathbf{e}} \rangle, \forall \check{\mathbf{e}} \in E, \tag{4.1}$$

where $\langle \cdot, \cdot \rangle$ denotes the duality pairing between E and E'. We have

$$\begin{aligned} \langle \Lambda \mathbf{e}, \check{\mathbf{e}} \rangle &= \int_\Omega \left[\psi_t(x,0)\check{\phi}(x,0) - \psi(x,0)\check{\phi}_t(x,0) \right] dx \\ &= \int_\Sigma \left[\frac{\partial \phi}{\partial n} \frac{\partial \check{\phi}}{\partial n} \right] d\Gamma \, dt, \forall \mathbf{e}, \check{\mathbf{e}} \in E. \end{aligned}$$

Hence the bilinear functional $\langle \Lambda \cdot, \cdot \rangle$ is continuous, symmetric and E-elliptic if the geometrical conditions of Theorem 3.1 are satisfied. This implies that for T large enough, problem (4.1) and hence $\Lambda \mathbf{e} = \mathbf{f}$ can be solved by a conjugate gradient algorithm.

Problem (4.1) is a particular case of:

$$\text{Find } u \in V \text{ such that } a(u,v) = L(v), \forall v \in V, \tag{4.2}$$

where, in the linear variational problem (4.2), we have

- V is a real Hilbert space for the scalar product $(\cdot, \cdot)$ and the corresponding norm $\|\cdot\|$;
- $a : V \times V \to \mathbb{R}$ is bilinear, continuous, symmetric and V-elliptic (or coercive);
- $L : V \to \mathbb{R}$ is linear and continuous.

Under these hypotheses, problem (4.2) has a unique solution which can be computed by the following conjugate gradient algorithm (which we will subsequently apply to our control problem):

Algorithm CG-0

Step 0. Initialization:

- $u^0 \in V$ is given;
- calculate the residual $g^0 \in V$ by solving

$$(g^0, v) = a(u^0, v) - L(v), \forall v \in V\,;$$

- if $g^0 = 0$ or is small, set $u = u^0$ and STOP; if not, set the first search direction $w^0 = g^0$ (steepest descent).

Then for $k = 0, 1, 2, \ldots$ assuming that u^k, g^k, w^k (solution, residual, search direction) are known, compute the next iterates u^{k+1}, g^{k+1}, w^{k+1} as follows:

Step 1. Descent:

- minimize (4.2) in the search direction by calculating

$$\rho_k = \frac{\|g^k\|^2}{a(w^k, w^k)}\,;$$

- update the solution

$$u^{k+1} = u^k - \rho_k w^k\,;$$

Step 2. Convergence test & new descent direction:

- calculate the residual $g^{k+1} \in V$ by solving

$$(g^{k+1}, v) = (g^k, v) - \rho_k a(w^k, v), \forall v \in V\,;$$

- if $g^{k+1} = 0$ or is small, set $u = u^{k+1}$ and STOP; if not, calculate

$$\gamma_k = \frac{\|g^{k+1}\|^2}{\|g^k\|^2}\,;$$

- define the new conjugate search direction as

$$w^{k+1} = g^{k+1} + \gamma_k w^k\,;$$

- set $k = k + 1$ and go to step 1.

4.2. Application of CG algorithm to the boundary control problem

We now apply Algorithm CG-0 to the solution of the boundary control problem for the wave equation (2.1) in the variational form (4.1). We recall the form of the space E and its dual

$$E = H_0^1(\Omega) \times L^2(\Omega), E' = H^{-1}(\Omega) \times L^2(\Omega),$$

and define the following inner product and norm on E:

$$(v, w)_E = \int_\Omega \left[\nabla v^0 \nabla w^0 + v^1 w^1\right] dx, \tag{4.3}$$

$$\|e\|_E^2 = \int_\Omega \left[\left|\nabla e^0\right|^2 + \left|e^1\right|^2\right] dx. \tag{4.4}$$

Now, we simply replace the functionals a and L in (4.2) by the corresponding terms of our exact controllability problem:

$$\begin{aligned} V &= E, \\ a(\cdot,\cdot) &= \langle \Lambda \cdot, \cdot \rangle, \\ L &: \check{\mathbf{e}} \to \langle \{u^1, -u^0\}, \mathbf{e} \rangle. \end{aligned}$$

We would like to point out a common source of confusion: the positive definite operator Λ is composed of the solution of the *two* wave equations in ϕ and ψ. Thus we *never* end up with a simple positive definite matrix (after discretization) as would be the case in the solution of a large linear system by conjugate gradient methods. In particular, we cannot measure directly the condition number of our operator. This need arises when we solve problems in which the geometrical conditions for controllability are not satisfied.

We obtain the following conjugate gradient algorithm (as introduced in [6] and [7]) for the exact controllability problem:

Algorithm CG-HUM

Step 0. Initialization:

- $e_0^0 \in H_0^1(\Omega)$, $e_1^0 \in L^2(\Omega)$ are given;
- calculate the residual $\mathbf{g}_0 = \{g_0^0, g_0^1\} \in E$ by solving
  - forwards in time

$$\begin{aligned} \Box \phi_0 &= 0 \text{ in } Q = \Omega \times (0,T), \\ \phi_0(x,0) = e_0^0, \frac{\partial \phi_0}{\partial t}(x,0) &= e_0^1 \text{ in } \Omega, \\ \phi_0(x,t) &= 0 \text{ on } \Gamma \times (0,T) = \Sigma\,; \end{aligned} \tag{4.5}$$

  - then backwards from $t = T$ to $t = 0$

$$\begin{aligned} \Box \psi_0 &= 0 \text{ in } Q = \Omega \times (0,T), \\ \psi_0(x,T) = 0, \frac{\partial \psi_0}{\partial t}(x,T) &= 0 \text{ in } \Omega, \\ \psi_0(x,t) &= 0 \quad \text{on } \Sigma \setminus \Sigma_0 = \Gamma \setminus \Gamma_0 \times (0,T)\,; \end{aligned} \tag{4.6}$$

  - finally,

$$\begin{aligned} -\Delta g_0^0 &= \frac{\partial \psi_0}{\partial t} - u^1 \text{ in } \Omega, \\ g_0^0 &= 0 \text{ on } \Gamma, \end{aligned} \tag{4.7}$$

    with

$$g_0^1 = u^0 - \psi_0(x,0) \text{ in } \Omega\,;$$

- if $\mathbf{g}_0 = 0$ or is small, set $\mathbf{e} = \mathbf{e}_0$ and STOP; if not, set the first search direction $\mathbf{w}_0 = \mathbf{g}_0$ (steepest descent).

Then for $k = 0, 1, 2, \ldots$ assuming that $\mathbf{e}_k$, $\mathbf{g}_k$, $\mathbf{w}_k$ are known, compute the next iterates $\mathbf{e}_{k+1}$, $\mathbf{g}_{k+1}$, $\mathbf{w}_{k+1}$ as follows:

Step 1. Descent:

- minimize (4.1) in the search direction by calculating

$$\rho_k = \frac{\|\mathbf{g}_k\|_E^2}{\langle \Lambda \mathbf{w}_k, \mathbf{w}_k \rangle} = \frac{\|\mathbf{g}_k\|_E^2}{(\bar{\mathbf{g}}_k, \mathbf{w}_k)_E},$$

where $\bar{\mathbf{g}}_k = \{\bar{g}_k^0, \bar{g}_k^1\}$ is obtained by solving

– forwards in time

$$\begin{aligned} \Box \bar{\phi}_k &= 0 \text{ in } Q = \Omega \times (0,T), \\ \bar{\phi}_k(x,0) = w_0^0, \frac{\partial \bar{\phi}_k}{\partial t}(x,0) &= w_0^1 \text{ in} \Omega, \\ \bar{\phi}_k(x,t) &= 0 \text{ on } \Gamma \times (0,T) = \Sigma\,; \end{aligned} \tag{4.8}$$

– then backwards from $t = T$ to $t = 0$

$$\begin{aligned} \Box \bar{\psi}_k &= 0 \text{ in } Q = \Omega \times (0,T), \\ \bar{\psi}_k(x,T) = 0, \frac{\partial \bar{\psi}_k}{\partial t}(x,T) &= 0 \text{ in } \Omega, \\ \bar{\psi}_k(x,t) &= 0 \quad \text{on } \Sigma \setminus \Sigma_0 = \Gamma \setminus \Gamma_0 \times (0,T)\,; \end{aligned} \tag{4.9}$$

– finally,

$$\begin{aligned} -\Delta \bar{g}_k^0 &= \frac{\partial \bar{\psi}_k}{\partial t} \text{ in } \Omega, \\ \bar{g}_k^0 &= 0 \text{ on } \Gamma, \end{aligned} \tag{4.10}$$

with

$$\bar{g}_k^1 = -\bar{\psi}_k(x,0) \text{ in } \Omega\,;$$

- update all quantities

$$\begin{aligned} \mathbf{e}_{k+1} &= \mathbf{e}_k - \rho_k \mathbf{w}_k, \\ \phi_{k+1} &= \phi_k - \rho_k \bar{\phi}_k, \\ \psi_{k+1} &= \psi_k - \rho_k \bar{\psi}_k, \\ \mathbf{g}_{k+1} &= \mathbf{g}_k - \rho_k \bar{\mathbf{g}}_k. \end{aligned}$$

Step 2. Convergence test & new descent direction:

- if $\mathbf{g}_{k+1} = 0$ or is small, set $\mathbf{e} = \mathbf{e}_{k+1}$, $\phi = \phi_{k+1}$, $\psi = \psi_{k+1}$ and STOP;
- else
  - calculate

$$\gamma_k = \frac{\|\mathbf{g}_{k+1}\|_E^2}{\|\mathbf{g}_k\|_E^2}\,;$$

  - define the new conjugate search direction as

$$\mathbf{w}_{k+1} = \mathbf{g}_{k+1} + \gamma_k \mathbf{w}_k\,;$$

- set $k = k + 1$ and go to step 1.

REMARK 4.1. Note that in the above conjugate gradient algorithm we seek (by minimization of the residual) the good initial conditions, e^0, e^1 of the ϕ wave equation – *not* those of the our original u wave equation. Once we have obtained these initial conditions, we can solve the ϕ wave equation and

calculate the boundary control $g = \frac{\partial \phi}{\partial n}|_{\Sigma_0}$ for the ψ wave equation. However, we imposed the conditions

$$\psi(x,T) = \psi_t(x,T) = 0.$$

Thus the solution of the ψ wave equation, using the *converged* value of g, will give us the exact controllability by simple identification with the u wave equation. The only role played by the initial conditions of u is in the calculation of the residue in the zeroth iteration of the conjugate gradient – see above.

We will make further remarks concerning the complexity of this algorithm at the end of the following section.

4.3. The discretization of the CG algorithm using a multigrid filtering technique

The discretization of the above algorithm has undergone numerous metamorphoses. The reason for this is the fact that a direct discretization leads to an *ill-posed* discrete problem. Numerous attempts were subsequently made in order to remedy this: see [7] and others. The most successful of these remedies was formulated by Glowinski in [6] and uses a multigrid filtering technique inspired from a similar problem which arises in the numerical solution of the Stokes problem. We now present a finite difference implementation of this technique. For the interested reader, a finite element implementation is given in the original paper [6].

The ill-posedness comes from the high frequency components of the solution of the discrete problem

$$\Lambda_{h,\triangle t}\mathbf{e}_h = \mathbf{f}_h.$$

The remedy (see [6] for analysis and details) is to eliminate the short wavelength components of the initial conditions of the ϕ wave equation by defining them on a coarse finite difference grid of twice the step-size, $2h$.

We will require two operators for the passage from grid to grid:

- an interpolation operator and
- an injection operator.

The interpolation operator maps the coarse grid onto the fine grid:

$$I_{2h}^{h} : \Omega^{2h} \longrightarrow \Omega^{h}$$

and is defined by

$$\begin{aligned}
\phi^h_{2i,2j} &= \phi^{2h}_{ij} \\
\phi^h_{2i+1,j} &= \frac{1}{2}\left(\phi^{2h}_{ij} + \phi^{2h}_{i+1,j}\right) \\
\phi^h_{i,2j+1} &= \frac{1}{2}\left(\phi^{2h}_{ij} + \phi^{2h}_{i,j+1}\right) \\
\phi^h_{2i+1,2j+1} &= \frac{1}{4}\left(\phi^{2h}_{ij} + \phi^{2h}_{i+1,j} + \phi^{2h}_{i,j+1} + \phi^{2h}_{i+1,j+1}\right)
\end{aligned}$$

for $0 \leq i,j \leq I/2 - 1$ where I is the number of elements in the fine grid. The injection operator maps the fine grid into the coarse:

$$I_{h}^{2h} : \Omega^{h} \longrightarrow \Omega^{2h}$$

by simply assigning the fine grid values to the corresponding coarse grid points

$$\phi^{2h}_{i,j} = \phi^{h}_{2i-1,2j-1}$$

for $i, j = 1, \ldots, I-1$.

We will now describe the conjugate gradient solution of the approximate problem. The discrete space, E_h, which approximates E is simply defined on the discrete domain Ω_{2h} at the points of the finite difference mesh. The $L^2(\Omega)$ inner product, $(\cdot,\cdot)_h$ is defined by a trapezoid integration over the discrete domain.

We approximate the fundamental equation $\Lambda \mathbf{e} = \mathbf{f}$ by the following linear variational problem in E_h:

$$\textit{Find } \mathbf{e}_h \in E_h \textit{such that}$$

$$\langle \Lambda_{h,\triangle t} \mathbf{e}_h, \varepsilon_h \rangle_h = \langle u^1, \varepsilon^0_h \rangle - \int_\Omega u^0 \varepsilon^1_h \, dx, \forall \varepsilon_h = \{\varepsilon^0_h, \varepsilon^1_h\} \in E_h, \qquad (4.11)$$

where $\langle \cdot, \cdot \rangle$ denotes the duality pairing between $H^{-1}(\Omega)$ and $H^1_0(\Omega)$. It can be shown (see [6, 7]) that the discrete operator $\langle \Lambda_{h,\triangle t} \cdot, \cdot \rangle$ is symmetric and positive definite for T large enough, and hence problem (4.11) can be solved by a conjugate gradient algorithm operating in E_h.

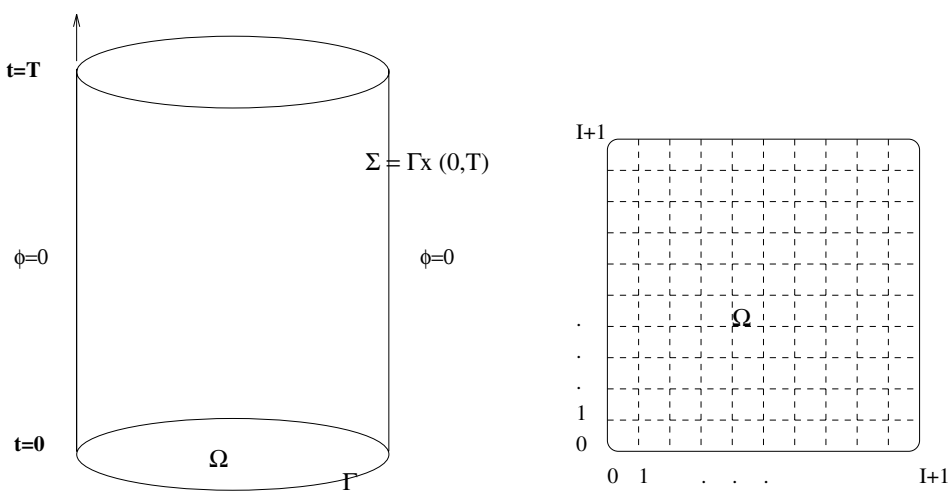

FIGURE 1. Discrete space-time domain for solution of $\Box\phi = 0$.

We now describe this algorithm. Suppose (to fix ideas) that $\Omega = (0,1) \times (0,1)$ and let the number of elements in each coordinate direction of the fine grid be I (see Figure 1). Let the space discretization, $h = 1/(I+1)$, and the time discretization, $\triangle t = T/N$, where T is the final time and N is the number of time steps. In order to satisfy the stability condition of the finite difference scheme, we must have $\triangle t \leq h/\sqrt{2}$. A point in Ω_h will be denoted $M_{ij} = \{ih, jh\}$ where $i, j = 1, 2, \ldots, I+1$. Then $\phi^n_{ij} = \phi(M_{ij}, n\Delta t)$. The

finite difference approximation of the ϕ wave equation is

$$\left\{\begin{array}{l} \dfrac{\phi_{ij}^{n+1}-2\phi_{ij}^{n}+\phi_{ij}^{n-1}}{(\triangle t)^2}-\Delta_h\phi^n=0 \text{ for } 1\le i,j\le I, 0\le n\le N,\\ \phi_{ij}^{0}=e^0(M_{ij}), \phi_{ij}^{1}-\phi_{ij}^{-1}=2\triangle t\, e^1(M_{ij}) \text{ for } 1\le i,j\le I, n=0,\\ \phi_{kl}^{n}=0 \text{ for } M_{kl}\in\Gamma, 0\le n\le N, \end{array}\right. \tag{4.12}$$

where Δ_h is the discrete 5-point Laplacian operator. The finite difference approximation of the ψ wave equation which is solved backwards from $t=T$ to $t=0$ is

$$\left\{\begin{array}{l} \dfrac{\psi_{ij}^{n-1}-2\psi_{ij}^{n}+\phi_{ij}^{n+1}}{(\triangle t)^2}-\Delta_h\psi^n=0 \text{ for } 1\le i,j\le I, n=N,\dots,0,\\ \psi_{ij}^{N}=0, \dfrac{\psi_{ij}^{N+1}-\psi_{ij}^{N-1}}{2\triangle t}=0 \text{ for } 1\le i,j\le I, n=N,\\ \psi_{kl}^{n}=\left\{\begin{array}{ll} \delta\phi_{kl} & \text{for } M_{kl}\in\Gamma_0, 0\le n\le N,\\ 0 & \text{for } M_{kl}\in\Gamma\setminus\Gamma_0, 0\le n\le N, \end{array}\right. \end{array}\right. \tag{4.13}$$

where the approximation to the normal derivative $\frac{\partial\phi}{\partial n}|_\Sigma=\delta\phi$ is defined by a second order difference (see Figure 2)

$$\delta\phi_{kl}=\frac{\partial\phi}{\partial n}(M_{kl})=\frac{\phi(E)-\phi(W)}{2h}.$$

Now, $\phi_{tt}=0$ implies $\Delta\phi=0$ on Σ. So

$$\frac{\phi(W)+\phi(E)+\phi(S)+\phi(N)-4\phi(M)}{h^2}=0,$$

which gives $\phi(E)=-\phi(W)$ (since everything else is zero on the boundary) and hence we obtain

$$\delta\phi_{kl}=\frac{\partial\phi}{\partial n}(M_{kl})=\frac{\phi(M)-\phi(W)}{h}. \tag{4.14}$$

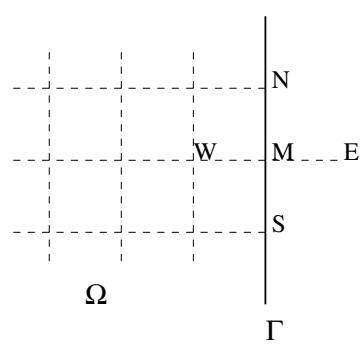

FIGURE 2. Discrete approximation to the normal derivative $\partial\phi/\partial n$.

The discrete algorithm is then:

Algorithm CG-h

Step 0. Initialization:

- e_0^0, e_0^1 are given on the *coarse* grid;
- solve the discrete forward wave equation (4.12) for $n = 0, 1, \ldots, N$ on the *fine* grid, initialized by

$$\phi_0^0 = I_{2h}^h e^0, \phi_0^1 - \phi_0^{-1} = (2\triangle t)\, I_{2h}^h e_0^1,$$

  and store ϕ_0^N and ϕ_0^{N+1};
- for $n = N, N-1, \ldots, 0$ compute ϕ_0^n, $\delta\phi_0^n$, ψ_0^{n-1} by integrating *backwards* in time as follows:
  - if $n = N$, compute $\delta\phi_0^N$ using (4.14);
  - else $(n < N)$
    - first compute ϕ_0^n by solving for one time step backwards on the *fine* grid

$$\frac{\phi_0^n - 2\phi_0^{n+1} + \phi_0^{n+2}}{(\triangle t)^2} - \Delta_h \phi_0^n = 0 \text{ for } 1 \le i, j \le I$$

      initialized by the stored values ϕ_0^N and ϕ_0^{N+1};
    - then $\delta\phi_0^n$ using (4.14);
  - endif;
  - solve (4.13) on the *fine* grid for ψ_0^{n-1} using $\psi_0^n = \delta\phi_0^n$ on Γ_0;
- calculate the residual $\mathbf{g}_0 = \{g_0^0, g_0^1\} \in E_h$ by
  - solving on the *coarse* grid

$$-\Delta_h g_0^0 = I_h^{2h} \frac{\psi_0^1 - \psi_0^{-1}}{2\triangle t} - I_h^{2h}\, u^1 \text{ for } 1 \le i, j \le I, \tag{4.15}$$
$$g_0^0 = 0 \text{ for } M_{ij} \in \Gamma;$$

  - then setting

$$g_0^1 = I_h^{2h} u^0 - I_h^{2h} \psi_0^0 \text{ for } 0 \le i, j \le I + 1\,;$$

- if $\mathbf{g}_0 = 0$ or is small, set $\mathbf{e}_h = \mathbf{e}_0$ and STOP; if not, set the first search direction $\mathbf{w}_0 = \mathbf{g}_0$ (steepest descent).

Then for $k = 0, 1, 2, \ldots$ assuming that $\mathbf{e}_k$, $\mathbf{g}_k$, $\mathbf{w}_k$ are known, compute the next iterates $\mathbf{e}_{k+1}$, $\mathbf{g}_{k+1}$, $\mathbf{w}_{k+1}$ as follows:

Step 1. Descent:

- solve the discrete forward wave equation (4.12) for $\bar{\phi}_k^n$, on the *fine* grid $n = 0, \ldots, N$, initialized by

$$\bar{\phi}_k^0 = I_h^{h/2} w_k^0, \bar{\phi}_k^1 - \bar{\phi}_k^{-1} = (2\triangle t)\, I_h^{h/2} w_k^1$$

  and store $\bar{\phi}_k^N$ and $\bar{\phi}_k^{N+1}$;
- for $n = N, N-1, \ldots, 0$ compute $\bar{\phi}_k^n$, $\delta\bar{\phi}_k^n$, $\bar{\psi}_k^{n-1}$ by integrating *backwards* in time as follows:
  - if $n = N$, compute $\delta\bar{\phi}_k^N$ from $\bar{\phi}_k^N$ using (4.14);
  - else $(n < N)$

* first compute $\bar{\phi}_k^n$ by solving for one time step backwards on the *fine* grid

$$\frac{\bar{\phi}_k^n - 2\bar{\phi}_k^{n+1} + \bar{\phi}_k^{n+2}}{(\triangle t)^2} - \Delta_h \bar{\phi}_k^n = 0 \text{ for } 1 \leq i,j \leq I$$

initialized by the stored values $\bar{\phi}_k^N$ and $\bar{\phi}_k^{N+1}$;

* then $\delta\bar{\phi}_k^n$ from $\bar{\phi}_k^n$ using (4.14);

– endif;

– solve (4.13) on the *fine* grid for $\bar{\psi}_k^{n-1}$ using $\psi_0^n = \delta\bar{\phi}_0^n$ on Γ_0;

- calculate the residual $\bar{\mathbf{g}}_k = \{\bar{g}_k^0, \bar{g}_k^1\} \in E_h$ by

– solving on the *coarse* grid

$$-\Delta_h \bar{g}_k^0 = I_h^{2h} \frac{\bar{\psi}_k^1 - \bar{\psi}_k^{-1}}{2\triangle t} \text{ for } 1 \leq i,j \leq I, \tag{4.16}$$

$$\bar{g}_k^0 = 0 \text{ for } M_{ij} \in \Gamma;$$

– then setting

$$g_0^1 = -I_h^{2h} \bar{\psi}_k^0 \text{ for } 0 \leq i,j \leq I+1;$$

- minimize (4.11) in the search direction by calculating

$$\rho_k = \frac{\|\mathbf{g}_k\|_{E_h}^2}{\langle \Lambda \mathbf{w}_k, \mathbf{w}_k \rangle_h} = \frac{\|\mathbf{g}_k\|_{E_h}^2}{(\bar{\mathbf{g}}_k, \mathbf{w}_k)_{E_h}},$$

where the inner product and norm are the discrete analogues (obtained by trapezoid integration) of (4.3) and (4.4) respectively;

- update all quantities

$$\mathbf{e}_{k+1} = \mathbf{e}_k - \rho_k \mathbf{w}_k,$$
$$\phi_{k+1} = \phi_k - \rho_k \bar{\phi}_k,$$
$$\psi_{k+1} = \psi_k - \rho_k \bar{\psi}_k,$$
$$\mathbf{g}_{k+1} = \mathbf{g}_k - \rho_k \bar{\mathbf{g}}_k.$$

Step 2. Convergence test and new descent direction:

- if $\mathbf{g}_{k+1} = 0$ or is small, set $\mathbf{e} = \mathbf{e}_{k+1}$, $\phi = \phi_{k+1}$, $\psi = \psi_{k+1}$ and STOP;
- else

– calculate

$$\gamma_k = \frac{\|\mathbf{g}_{k+1}\|_{E_h}^2}{\|\mathbf{g}_k\|_{E_h}^2};$$

– define the new conjugate search direction as

$$\mathbf{w}_{k+1} = \mathbf{g}_{k+1} + \gamma_k \mathbf{w}_k;$$

- set $k = k+1$ and go to step 1.

REMARK 4.2. We repeat here two basic remarks made in [6] concerning the complexity of the above discrete algorithm:

1. "The above algorithm may seem complicated at first glance [...] but the only non-trivial part of it is the solution (on the coarse grid) of the discrete Dirichlet problems (4.15) and (4.16). An interesting feature of the algorithm is that the simultaneous backward integration (in the descent step) of the 2 discrete wave equations for ϕ and ψ provides a

very substantial computer memory saving [...] The saving would be more substantial for large T and would be an absolute necessity for 3-d problems."

2. The above remark also shows the interest of the HUM approach from a computational point of view. In the original control problem, the unknown is the control g which is defined over $\Sigma_0 = \Gamma_0 \times (0,T)$; using the HUM, the unknown is the solution $\mathbf{e}$ of $\Lambda \mathbf{e} = \mathbf{f}$ which is approximated by $\mathbf{e}_h$ and is substantially smaller in terms of memory requirement.

5. Norms of the control g and the energetic cost of control

The following discussion is in fact related to the numerical results presented in the following section. We examine here the relationship between the norm of the control g and the control time T.

5.1. Norms of control

The HUM is formulated in such a way that the control obtained minimizes the objective function

$$J(g;T) = \frac{1}{2} \int_{\Sigma_0} |g|^2 \, d\Sigma,$$

where $\Sigma_0 = \Gamma_0 \times (0,T)$. This is an L^2 norm which we denote $\|g\|^2_{2,\Sigma_0}$. We define an L^1 norm of g as follows:

$$\|g\|_{1,\Sigma_0} = \int_0^T \left(\int_{\Gamma_0} |g|^2 \, dx \right)^{1/2} dt = \int_0^T \|g(t)\|_{L^2(\Gamma_0)} \, dt.$$

This is the standard $L^1(0,T;L^2(\Gamma_0))$ norm. The results of the simulations on the unit square are shown in Figure 4, where we compare the quantities: $\|g\|_{2,\Sigma_0}$ (denoted as L^2 norm), $\sqrt{T}\|g\|_{2,\Sigma_0}$ and $\|g\|_{1,\Sigma_0}$ (denoted as L^1 norm) as functions of T.

We observe the following (see Figure 4 and also Figures 6, 9 and 16): the L^2 norm is a decreasing function of T, whereas the L^1 norm is approximately *constant* and thus independent of T. On multiplying the L^2 norm by the square root of T, we obtain a behavior similar to that of the L^1 norm. It was already noted in [7] that

$$\sqrt{T}\|g\|_{2,\Sigma_0} \sim c,$$

but we can see now that the constant c is closely related to the L^1 norm, $\|g\|_{1,\Sigma_0}$. In fact, our observations lead us to a relation

$$\sqrt{T}\|g\|_{2,\Sigma_0} = \|g\|_{1,\Sigma_0} + c\,, \tag{5.1}$$

where c is a positive constant. We are thus led to propose the $L^1(0,T;L^2(\Gamma_0))$ norm as a cost function for the HUM.

5.1.1. THE 1-D CASE. We can investigate the above relation in the very special case of one space dimension. We consider the "vibrating string" described by

$$\begin{aligned} u_{tt} - u_{xx} = 0 \quad &\text{in } 0 < x < 1, \\ u(0,t) = g(t)\ ,\ u(1,t) &= 0\ , \\ u(x,0) = a(x)\ ,\ u_t(x,0) &= b(x)\ , \end{aligned} \tag{5.2}$$

where the functions a and b are given in $L^2 \times H^{-1}$ and $g(t)$ is the control function. The solution of (5.2) is of the form

$$u(x,t) = \phi(t-x) + \psi(t+x),$$

where (ϕ, ψ) satisfy the relations

$$\begin{aligned} \phi(-x) + \psi(x) &= a(x), \quad \phi'(-x) + \psi'(x) = b(x), \quad 0 < x < 1, \\ \phi(t-1) + \psi(t+1) &= 0, \quad \forall t \in \mathbb{R}, \\ g(t) &= \phi(t) + \psi(t), \quad \forall t \in \mathbb{R}. \end{aligned}$$

From the above relations we deduce that $\psi(t) = -\phi(t-2)$ and that

$$\begin{aligned} \phi(-x) - \phi(x-2) &= a(x), \quad 0 < x < 1, \\ \phi'(-x) - \phi'(x-2) &= b(x), \quad 0 < x < 1. \end{aligned} \tag{5.3}$$

Thus $\phi(t)$ is given up to a constant in the interval $t \in (-2, 0)$, and the control function g satisfies

$$g(t) = \phi(t) - \phi(t-2). \tag{5.4}$$

In particular, the set G of control functions g with support in $[0,T]$, driving (5.2) to rest at time T,

$$G = \left\{ g \in L^2(0,T)\ ;\ \text{the solution } u(x,t) \text{ of (5.2) is 0 for } t > T \right\},$$

is equal to

$$G = \{ g(t) = \phi(t) - \phi(t-2)\ ;\ \phi \in \Phi \}$$

with

$$\Phi = \left\{ \phi \in L^2(-2,T)\ ;\ \phi|_{t>T-2} = 0\ ,\ \phi|_{t<0} = \phi_0 \right\},$$

where ϕ_0 is the solution of (5.3).

Taking $T = 2(N+1)$ with N an integer, and denoting by ϕ_j the function on $(0,2)$ given by $\phi_j(t) = \phi(t + 2(j-1))$ for $0 \le j \le N$, we have (with $\phi_{N+1} \equiv 0$)

$$\begin{aligned} \|g\|^2_{L^2(0,T)} &= \sum_{j=1}^{N+1} \|\phi_j - \phi_{j-1}\|^2_{L^2(0,2)}, \\ \|g\|_{L^1(0,T)} &= \sum_{j=1}^{N+1} \|\phi_j - \phi_{j-1}\|_{L^1(0,2)}. \end{aligned}$$

In particular, the optimal control in $L^2(0,T)$, g_2, is unique and is characterized by

$$\phi_j = \phi_{j-1} - \frac{\phi_0}{N+1}\ , \quad 1 \le j \le N.$$

Thus we get

$$\inf\left\{\|g\|_{L^2(0,T)}\,;\,g\in G\right\}=\|g_2\|_{L^2(0,T)}=\frac{1}{\sqrt{N+1}}\|\phi_0\|_{L^2(-2,0)}.$$

On the other hand, the triangle inequality gives

$$\inf\left\{\|g\|_{L^1(0,T)}\,;\,g\in G\right\}=\|\phi_0\|_{L^1(-2,0)}=\|g_2\|_{L^1(0,T)}.$$

From these facts we conclude that for $T=2(N+1)$

$$\begin{aligned}\inf\left\{\|g\|_{L^1(0,T)}\,;\,g\in G\right\} &= \|\phi_0\|_{L^1(-2,0)}\\ &\le \sqrt{2}\|\phi_0\|_{L^2(-2,0)}=\sqrt{T}\inf\left\{\|g\|_{L^2(0,T)}\,;\,g\in G\right\}\end{aligned}$$

and the optimal L^2 control is also L^1 optimal. We observe also that the set of L^1 minimizers

$$\left\{g\in L^1(0,T)\,;\,\|g\|_{L^1(0,T)}=\|\phi_0\|_{L^1(-2,0)}\right\}$$

is infinite for $N\ge 1$ and that the choice $g_1=-\chi_{[0,2]}\phi_0(t-2)$ is both L^1 optimal and supported in the smallest possible time interval. Notice also that we obtain a relation of the type (5.1):

$$\sqrt{T}\|g_2\|_{L^2(0,T)}=\|g_1\|_{L^1(0,T)}+c,$$

where c is the constant

$$c=\sqrt{2}\|\phi_0\|_{L^2(-2,0)}-\|\phi_0\|_{L^1(-2,0)}\ge 0.$$

5.1.2. The general case – interior control. In order to try and explain (5.1) in the general case, we first consider the wave equation in $\mathbb{R}^2$ with an "interior" control, g, acting on $\omega\subset\Omega$

$$(\partial_t^2-c^2\Delta)u=g \text{ in } \Omega,$$

with the zero initial condition

$$u|_{t=0}=0,\qquad u_t|_{t=0}=0.$$

We then have the following energy estimate

$$\sqrt{E(u)(T)}\le\int_0^T\left(\int_\Omega g^2\,dx\right)^{1/2}dt.$$

This is easily obtained by rewriting the system in the form

$$(\partial_t-A)U=G$$

where

$$U=\begin{bmatrix}u\\ \frac{\partial u}{\partial t}\end{bmatrix},\ G=\begin{bmatrix}0\\ g\end{bmatrix}$$

and the operator A is defined by

$$A=\begin{bmatrix}0 & I\\ c^2\Delta & 0\end{bmatrix}.$$

This system then has the solution

$$U=\int_0^t \exp^{(t-s)A}G\,ds$$

and immediately gives the L^1 estimate

$$|U|_H \leq \int_0^t |G|_H \, ds.$$

5.1.3. Dimensional analysis. A *qualitative* justification of the suitability of this L^1 norm is given by the following dimensional analysis. Define the physical energy as

$$E = \int_\Omega |u_t|^2 + |c\nabla_x u|^2 \, dx,$$

then, denoting the dimensions of a quantity by $[\cdot]$, we want $[E] = \text{kg m}^2\text{s}^{-2}$. This implies that $[u] = \text{kg}^{1/2}$. Thus the dimension of the control must be $[g] = \text{kg}^{1/2}\text{s}^{-2}$. Now our L^1 norm,

$$\|g\|_{L^1} = \int_0^T \left(\int_\Omega g^2 \, dx \right)^{1/2} dt,$$

has a dimension (squared) of kg m^2 s^{-2} which is precisely that of $[E]$. However, the criterion optimized by the HUM

$$\|g\|_{L^2} = \left(\int_0^T \int_\Omega g^2 \, dx \, dt \right)^{1/2}$$

has a dimension (squared) of kg m^2 s^{-3} and this is an energy per unit time or a *power*. Physically then, it is reasonable that the power decreases as we extend the time interval, but it is the work that provides a better estimation of the *tota*l energy spent in controlling the system. Thus, extending the control interval $(0, T)$ leads to a decrease in the power (and consequently a more optimal solution in the $L^2(\Sigma)$ norm), but a constant expenditure of energy.

The graphs (see below) show that the L^1-norm is approximately constant. If we define

$$A = \sqrt{T}\|g\|_{L^2(\Sigma)}, B = \|g\|_{L^1(0,T;L^2(\Gamma))}$$

then since these two quantities have the same homogeneity, we have by the Cauchy-Schwarz inequality

$$B \leq A.$$

What we observe with our choice of data is that

$$B \sim A$$

and that both are approximately *constant*. This is striking since it implies that once we have found an optimal control, g, all other controls for larger T can be obtained directly from this one. This can be explained by the following argument. Suppose we have found a control (optimal) g_T such that

$$g_T : u(0) \to 0$$

in time T. Let us now extend the time axis from 0 to $2T$. Then by linearity the following control function will drive our system to rest:

$$g_{2T} = \begin{cases} \frac{1}{2}g_T, & 0 \le t < T \\ \frac{1}{2}g_T, & T \le t \le 2T\,. \end{cases}$$

The trivial estimation gives

$$\int_0^{2T}\int_\Gamma |g_{2T}|^2 \le \int_0^T\int_\Gamma \left|\frac{g_T}{2}\right|^2 + \int_T^{2T}\int_\Gamma \left|\frac{g_T}{2}\right|^2 = \frac{1}{2}\int_0^T\int_\Gamma |g_T|^2,$$

which implies that

$$\sqrt{2T}\left(\int_0^{2T}\int_\Gamma g_{2T}^2\right)^{1/2} \le \sqrt{T}\left(\int_0^T\int_\Gamma g_T^2\right)^{1/2}.$$

However, the quantity on the right is approximately constant in the simulations, *i.e.,* it is independent of T. Thus we must have equality in the above estimate. Hence for any extension of the time axis to $T' > T$, we can construct the new control based on the interval $[0, T]$ by linear combinations of g_T since all the control information is already contained in the function g_T .

5.1.4. The general case – boundary control. We have not yet discussed the case where g is on the boundary Γ. We have a difficulty in obtaining results analogous to the interior case due to the spaces in which g must lie. Here the problem is the following:

$$(\partial_t^2 - c^2\Delta)v = 0 \text{ in } \Omega,$$

with the non-zero boundary condition

$$v|_\Gamma = g, \tag{5.5}$$

where $g \in L^2(\Gamma)$. The solution $(v, v_t) \in (L^2, H^{-1})$. The dual problem

$$(\partial_t^2 - c^2\Delta)u = 0 \text{ in } \Omega$$

has its solution $(u, u_t) \in (H_0^1, L^2)$. Taking inner products and using the duality, we obtain

$$\int_0^T\int_\Omega < (\partial_t^2 - c^2\Delta)v, u >= \int_0^T\int_\Gamma g\partial_n u\,.$$

Now defining

$$E(u) = |u|^2_{H_1^0} + |u_t|^2_{L^2},$$

the fact that (5.5) is well-posed results from the estimate

$$c^2\int_0^T\int_\Gamma |\partial_n u|^2 \le CE(u),$$

where C is a constant. Our problem is thus well-posed with $v \in C([0,T], L^2)$ $\cap\, C^1([0,T], H^{-1})$ if $g \in L^2((0,T)\times\Gamma)$ but *not* if $g \in L^1(0,T; L^2(\Gamma))$, which is after all a good justification (at least for theoretical purposes) to work in $L^2(\Sigma)$.

5.1.5. Linear elasticity system. We note that also in the case of the linear elasticity system (see [3]) we consistently find that $\sqrt{T}\|g\|_{L^2(\Sigma)} \sim c$ and in fact the constant can be estimated numerically by simply setting $T = 1$. This is possible on condition that we have geometric controllability at time $t = 1$.

5.2. The energetic cost of control

First we introduce the following notation for the discrete norms:

- $\|\cdot\|_{1,\Sigma}$ is the $L^1(0,T\,;\,L^2(\Gamma))$ norm; $\|\cdot\|_{2,\Sigma}$ is the $L^2(\Sigma)$ norm;
- $\|\cdot\|_{2,\Omega}$ is the $L^2(\Omega)$ norm;
- $|\cdot|_{1,\Omega}$ is the $H_0^1(\Omega)$ norm;
- $\|\cdot\|_{-1,\Omega}$ is the $H^{-1}(\Omega)$ norm, where $\|v\|_{-1,\Omega} = |w|_{1,\Omega}$ with $|v|_{1,\Omega} = (\int_\Omega |\nabla v|^2\,dx)^{1/2}$ and $w \in H_0^1(\Omega)$ is the solution of the Dirichlet problem $-\Delta w = v$ in Ω, $w = 0$ on Γ.

As a result of the dependence of the norms of the control on the control time (T) as discussed above, and following the abstract analysis of Appendix A, we find it appropriate to introduce a new criterion for estimating the optimal quality of the solution obtained. We are led to the following

Definition 5.1 **(ECV, ECF).** The energetic cost vector (ECV) is defined as

$$\mathrm{ECV} = \left[\frac{\|g\|_{1,\Sigma}}{\|u^0\|_{2,\Omega}}, \frac{\|u(T)\|_{2,\Omega} + \|u_t(T)\|_{-1,\Omega}}{\|u^0\|_{2,\Omega}}\right]$$

and the energetic cost factor (ECF) is the product of its two components

$$\mathrm{ECF} = \left(\frac{\|g\|_{1,\Sigma}}{\|u^0\|_{2,\Omega}}\right)\left(\frac{\|u(T)\|_{2,\Omega} + \|u_t(T)\|_{-1,\Omega}}{\|u^0\|_{2,\Omega}}\right).$$

This factor takes into account the cost of applying the control (in the L^1 norm) as well as the cost incurred in driving the system to a final state which is close to zero. It is normalized by the norm of the initial data to allow comparison between different cases ("controllable" and "uncontrollable" data). The smaller the value of the components of the ECV, the better the quality of the solution which then has

1. a smaller control energy and
2. a final state closer to rest.

In the numerical results we will also present the ECF since it provides us with a useful scalar value and enables comparisons between cases with different geometries and initial conditions.

6. The wave equation on the unit square: numerical study

Before presenting the numerical results we will give an overview of the different geometrical configurations studied and discuss the convergence criterion and the discrete norms used. Other aspects of convergence are considered in Appendix C.

6.1. Geometry of domains and control boundaries

In the numerical simulations that follow, we study three geometrical situations – see Figure 3:

1. a square domain with varying control boundary;
2. squares with cavities giving rise to trapped rays;
3. an elliptical region which exhibits different stability properties along the minor and major axes.

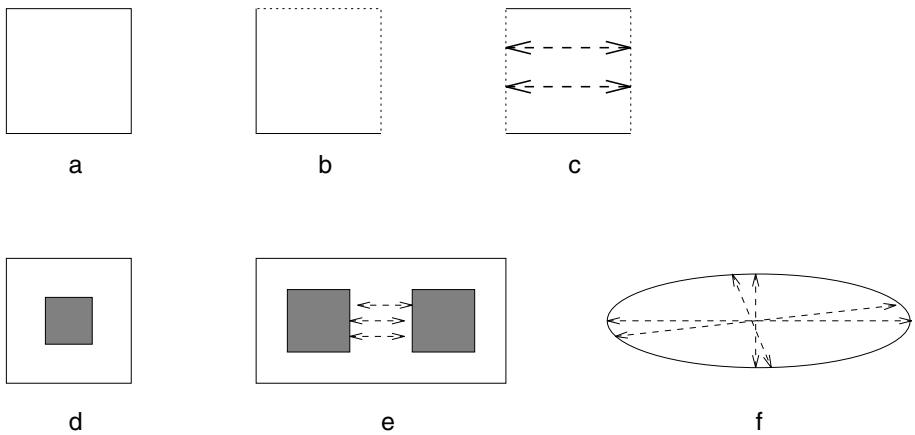

Figure 3. Geometries: squares (a,b,c), cavities (d,e) and ellipse (f) – no control on dotted boundaries; rays of geometric optics are indicated by thick arrows.

6.2. Convergence criterion and discrete norms

1. The conjugate gradient algorithm is initialized by $e_0^0 = e_0^1 = 0$. In other words, the initial guess to the solution $\mathbf{e}_h$ is zero.
2. The stopping criterion: we use
$$\frac{\|\mathbf{g}_{k+1}\|_{E_h}^2}{\|\mathbf{g}_0\|_{E_h}^2} \leq \varepsilon$$
where ε depends on the machine precision. In our calculations we use $\varepsilon = 10^{-6}$. On a supercomputer this precision can be increased to 10^{-12} as was done in [6]. In cases with oscillatory initial data (see below), we reduce this tolerance to 10^{-5} – this being the smallest value attainable in these cases. Examples can be found in Appendix C.
3. In the Tables we denote by u_c^0 and u_c^1 the calculated values of the initial conditions u^0 and u^1. They are in fact the discrete analogues of the converged values of $\psi(0)$ and $\frac{\partial \psi}{\partial t}(0)$.
4. We use the discrete norms defined in the previous section.
5. The quantity $\|g\|_{2,\Sigma}$ is the L^2 norm over time of $\|g(t)\|_{L^2(\Gamma_0)}$ – this last function is plotted against time and shows how the energy of the control varies in time.
6. The 2 quantities $\frac{\|u^0 - u_c^0\|_{2,\Omega}}{\|u^0\|_{2,\Omega}}$ and $\|u^1 - u_c^1\|_{-1,\Omega}$ measure how well the *initial* conditions of the original wave equation are recovered by the algorithm (recall that they are obtained from the ψ equation).

7. The 2 quantities $\frac{\|u(T)\|_{2,\Omega}}{\|u^0\|_{2,\Omega}}$ and $\|u_t(T)\|_{-1,\Omega}$ are obtained by solving the original wave equation for u, starting from the given initial data, and employing the exact boundary control, g, which has just been calculated by the algorithm. They show how well the calculated control achieves the desired *terminal* state $u(x,T) = u_t(x,T) = 0$.

Note that all norms involving the time derivative of u are not normalized since we use a zero initial condition on $\partial u/\partial t$.

6.3. The test problem

In order to verify the code, the test problem introduced in [7] was solved. This problem consists of an analytically obtained control acting on the boundary of the unit square. Results comparable to those of [6] were obtained. For a typical test run with $h = 1/32$, $\triangle t = h/\sqrt{2}$, $T = 2.65$ and $\varepsilon = 10^{-8}$, the algorithm converged after 24 iterations and the errors were

$$\left\|e^0 - e_c^0\right\|_{L^2(\Omega)} = 0.0059, \quad \left\|e^0 - e_c^0\right\|_{H^1(\Omega)} = 0.0103,$$
$$\left\|e^1 - e_c^1\right\|_{L^2(\Omega)} = 0.0649.$$

6.4. Initial data

In order to pursue our study of the geometrical aspects of controllability, we need a rather versatile function as the initial condition. We will take the following complex initial data for the wave equation:

$$\begin{aligned} u^0(x,y) &= u(x,y;0) = e^{-\alpha_x(x-x_0)^2-\alpha_y(y-y_0)^2+i[\beta_x(x-x_0)+\beta_y(y-y_0)]}, \quad (6.1)\\ u^1(x,y) &= \frac{\partial u}{\partial t}(x,y;0) = 0. \end{aligned}$$

We note the following properties of this function (see the various figures in the sequel):

- it has support centered around the point (x_0, y_0);
- the vector $\beta = (\beta_x, \beta_y)$ will give a preferred direction of propagation;
- the vector $\alpha = (\alpha_x, \alpha_y)$ will give support in a desired direction.

This function will enable us to study numerous phenomena:

- the dependence of the control on the direction $\beta = (\beta_x, \beta_y)$;
- the interaction between this direction and the geometry of the region as well as the geometry of the control boundary;
- oscillatory data which has "compact" support in one coordinate direction and rapid oscillation in the other.

6.5. Control on the entire boundary of the unit square

The results of the simulations using smooth initial data

$$u^0(x,y) = e^{-64[(x-x_0)^2+(y-y_0)^2]}, u^1(x,y) = 0,$$

with $(x_0, y_0) = (0.5, 0.5)$ are shown in Figure 4, where we compare the quantities: $\|g\|_{2,\Sigma}$ (the L^2 norm), $\sqrt{T}\|g\|_{2,\Sigma}$ and $\|g\|_{1,\Sigma}$ (the L^1 norm) as functions of T.

We observe the phenomenon referred to in the previous section (see Figure 4 and also Figures 6, 9 and 16): the L^2 norm is a decreasing function of

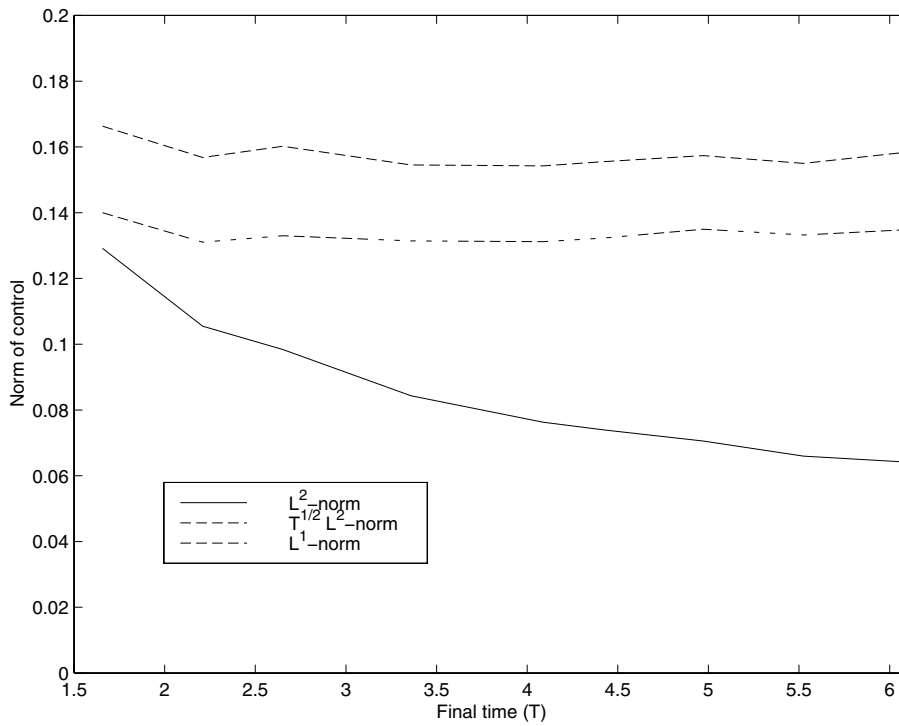

FIGURE 4. $L^1(0,T;L^2(\Gamma))$ and $L^2(\Sigma)$ norms of the boundary control as functions of the control time T for control on the entire boundary of a square.

T, whereas the L^1 norm is basically constant with a slight increase over T. On multiplying the L^2 norm by the square root of T, we obtain a behavior similar to that of the L^1 norm.

6.6. CONTROL ON A PART OF THE BOUNDARY OF THE UNIT SQUARE

Using the function (6.1) we will consider

- smooth, exponential initial data and
- oscillatory initial data.

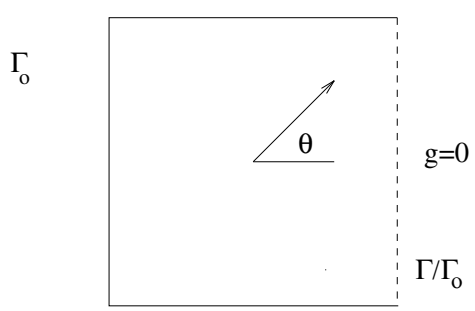

FIGURE 5. The square with zero control on eastern boundary.

6.6.1. EXPONENTIAL INITIAL DATA. The first series of runs (see Table 1) on the unit square shows the effect of the direction of β on the control. We consider two control geometries:

- control on the entire boundary, denoted by "■";
- control on the north, south and west boundaries, denoted by "⊏" ($g = 0$ on eastern boundary).

In all runs we set $\beta = (2, 0)$ and use a rotation of angle θ ($0 \leq \theta \leq \pi/2$) to change the direction of propagation of the initial data. For the ⊏-geometry we consider first the dependence on T for $\theta = 0$ fixed, then the dependence on θ for $T = 3.315$ fixed. These results are plotted in Figures 6 and 7 .

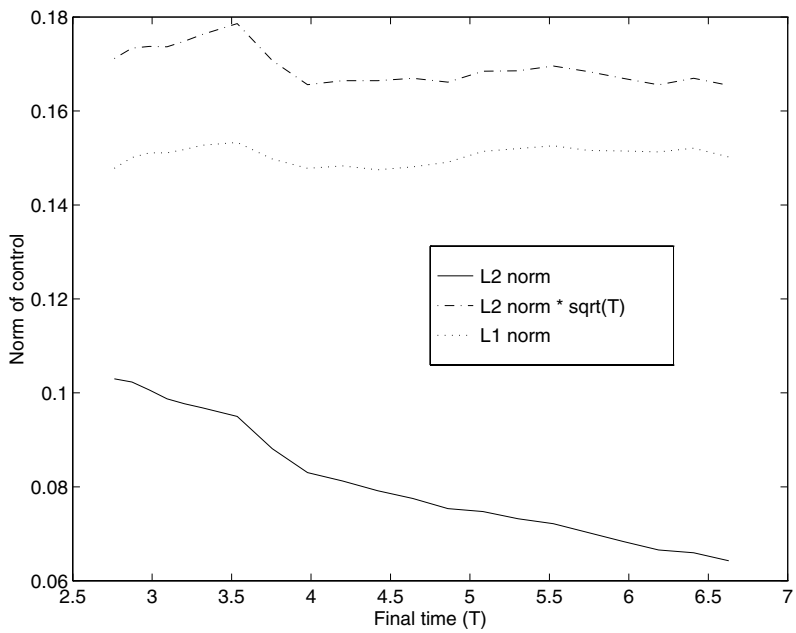

FIGURE 6. $L^1(0, T; L^2(\Gamma))$ and $L^2(\Sigma)$ norms of the boundary control as functions of the control time T for the open square ⊏.

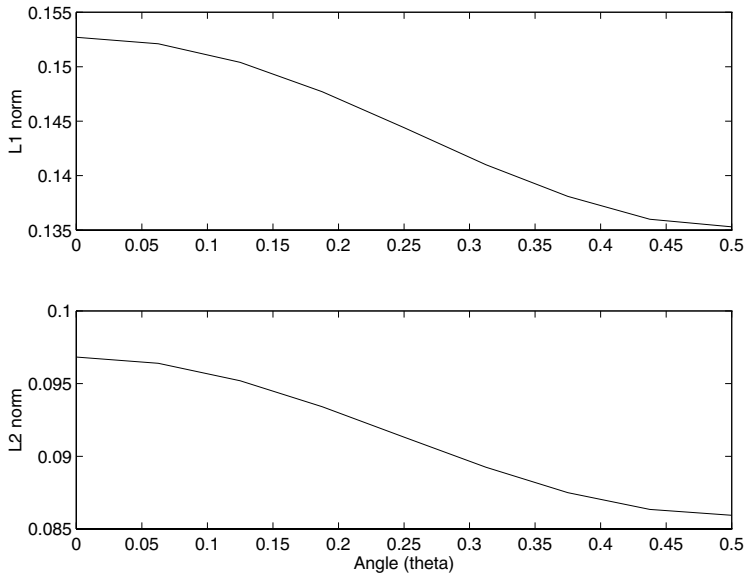

FIGURE 7. $L^1(0,T;L^2(\Gamma))$ and $L^2(\Sigma)$ norms of the boundary control as functions of the angle θ $(0 \leq \theta \leq \pi/2)$for the open square $\sqsubset$.

In the Table 1, we give detailed results of some of these simulations.

G	T	θ	$\|g\|_{2,\Sigma}$	$\|g\|_{1,\Sigma}$	$\frac{\|u^0-u_c^0\|_{2,\Omega}}{\|u^0\|_{2,\Omega}}$	$\frac{\|u(T)\|_{2,\Omega}}{\|u^0\|_{2,\Omega}}$	ECV	
■	1.44	0	0.0984	0.0926	0.045	0.045	$[0.59, 0.07] \Rightarrow 0.040$	
	1.44	$\frac{\pi}{4}$	0.0983	0.0926	0.044	0.044	$[0.59, 0.07] \Rightarrow 0.040$	(a)
$\sqsubset$	2.76	0	0.1030	0.1478	0.027	0.028	$[0.94, 0.05] \Rightarrow 0.043$	
	2.65	$\frac{\pi}{4}$	0.1009	0.1399	0.037	0.035	$[0.89, 0.06] \Rightarrow 0.053$	(b)
	2.21	$\frac{\pi}{2}$	0.1026	0.1287	0.023	0.024	$[0.82, 0.04] \Rightarrow 0.032$	
	2.87	0	0.1023	0.1501	0.025	0.026	$[0.96, 0.04] \Rightarrow 0.043$	
	3.76	0	0.0881	0.1498	0.026	0.028	$[0.96, 0.04] \Rightarrow 0.041$	
	4.42	0	0.0798	0.1475	0.022	0.019	$[0.94, 0.03] \Rightarrow 0.030$	(c)
	5.30	0	0.0732	0.1520	0.020	0.018	$[0.97, 0.03] \Rightarrow 0.031$	
	6.63	0	0.0643	0.1502	0.021	0.018	$[0.96, 0.03] \Rightarrow 0.027$	
	3.32	0	0.0968	0.1527	0.024	0.022	$[0.97, 0.04] \Rightarrow 0.039$	
	3.32	$\frac{\pi}{8}$	0.0952	0.1504	0.023	0.022	$[0.96, 0.04] \Rightarrow 0.038$	
	3.32	$\frac{\pi}{4}$	0.0913	0.1444	0.022	0.020	$[0.92, 0.04] \Rightarrow 0.033$	(d)
	3.32	$\frac{3\pi}{8}$	0.0875	0.1381	0.022	0.019	$[0.88, 0.03] \Rightarrow 0.029$	
	3.32	$\frac{\pi}{2}$	0.0859	0.1353	0.021	0.018	$[0.86, 0.03] \Rightarrow 0.027$	

TABLE 1. Complex data on the unit square with 2 control geometries; convergence criterion, $\varepsilon = 10^{-5}$; $\alpha = (64, 64)$; $\beta = (2, 0)$, $N = 32$. The ECV column gives its 2 components followed by their product. Notes: $^{(a)}$ T is minimal here; $^{(b)}$ the smallest T for control, varying θ; $^{(c)}$ for $\theta = 0$, dependence on T; $^{(d)}$ for $T = 3.32$, dependence on θ.

REMARK 6.1.

- We need less time to control from the entire boundary than from a part, as expected.
- As in the case of control on the entire boundary, it is the L^1 norm and hence the ECF which gives a better cost function – see Figure 6.
- When the direction of propagation is perpendicular to the uncontrolled boundary, the time needed to control increases when compared with the direction parallel. The case where the angle is $\pi/4$ is intermediate and there is a clear functional relationship between the 2 norms and the angle – see Figure 7.

6.6.2. OSCILLATORY INITIAL DATA. We now impose oscillatory initial data with compact support in the y-coordinate direction and rapid oscillation in the x-direction as shown in Figure 8. Note that this function is real. We consider two different geometries for the control boundary:

- control on the west and south boundaries, denoted by "L" – in this case we *have* geometric control;
- control on the north and south boundaries, denoted by "=" ($g = 0$ on eastern and western boundaries) – in this case there is *no* geometric control.

Detailed results are presented in Table 2. The norms are plotted in Figure 9.

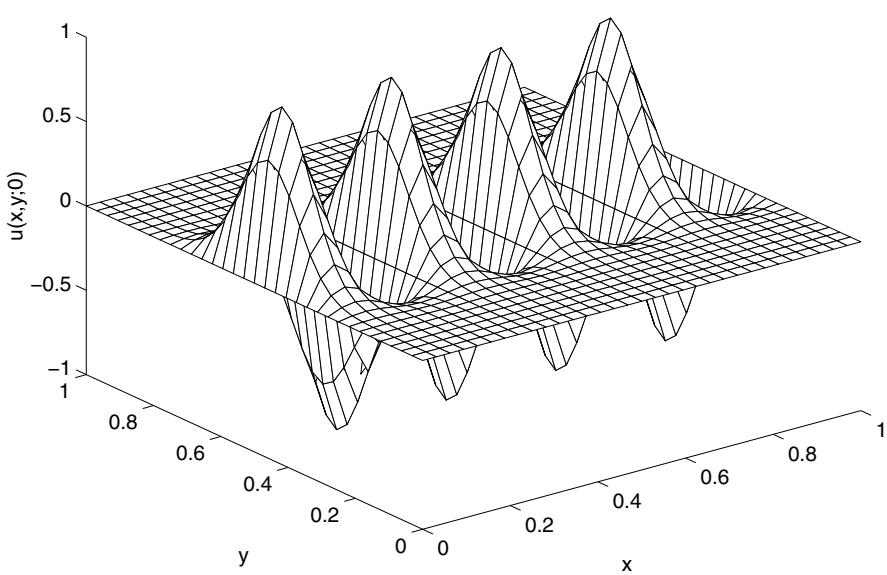

FIGURE 8. Oscillatory initial condition, compactly supported in y and rapidly oscillating in x. Notes: this function is the product $e^{-64(y-y_0)^2}\Re\left(e^{i8(x-x_0)}\right)$.

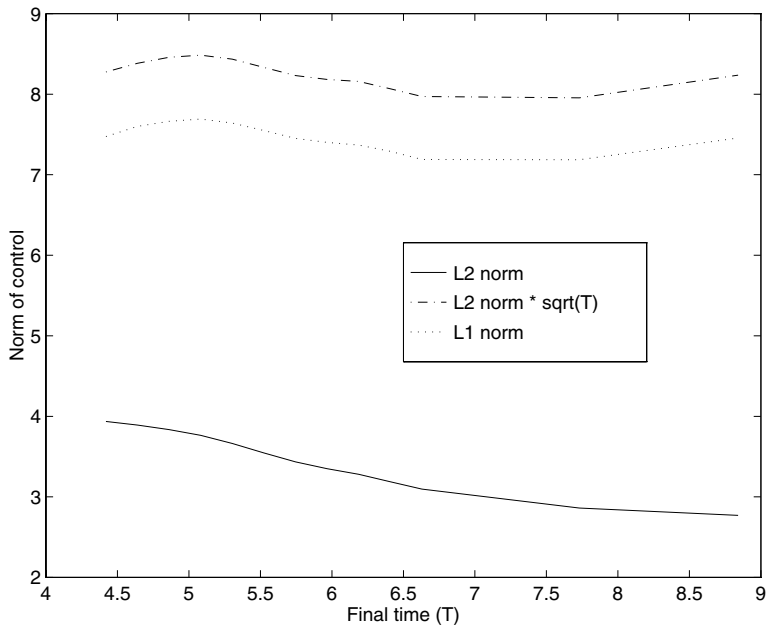

FIGURE 9. $L^1(0,T;L^2(\Gamma))$ and $L^2(\Sigma)$ norms of the boundary control as functions of the control time T for oscillatory initial condition on "=" control geometry.

G	T	$\|g\|_{2,\Sigma}$	$\|g\|_{1,\Sigma}$	$\frac{\|u^0-u_c^0\|_{2,\Omega}}{\|u^0\|_{2,\Omega}}$	$\frac{\|u(T)\|_{2,\Omega}}{\|u^0\|_{2,\Omega}}$	ECV	
L	4.42	0.1873	0.3771	0.080	0.062	$[1.35, 0.11] \Rightarrow 0.143$	(a)
=	4.42	3.937	7.475	0.139	0.120	$[26.7, 0.20] \Rightarrow 5.232$	
	4.86	3.836	7.663	0.181	0.164	$[27.4, 0.25] \Rightarrow 6.889$	
	5.74	3.434	7.451	0.149	0.135	$[26.6, 0.22] \Rightarrow 5.954$	(b)
	6.63	3.096	7.189	0.121	0.099	$[25.7, 0.16] \Rightarrow 3.992$	
	7.73	2.861	7.187	0.081	0.072	$[25.7, 0.12] \Rightarrow 3.051$	

TABLE 2. Oscillatory data on the unit square with 2 control geometries; $\alpha = (0, 64)$,$\beta = (8, 0)$, $\theta = 0$, $N = 32$. The ECV column gives its 2 components followed by their product. Notes: $^{(a)}$ convergence criterion $\varepsilon = 10^{-5}$, T is minimal; $^{(b)}$ $\varepsilon = 10^{-4}$ but not all runs converged – they were stopped at point where the convergence criterion started to increase (between 1 and $5 \cdot 10^{-4}$) – see Appendix B.

REMARK 6.2.

- If we compare with the results of Table 1 we see that the oscillatory data takes longer to control and approximately 20 times the energy; the final state is one order of magnitude larger and the overall ECF (energetic cost factor) is about 100 times larger.
- Comparing the 2 cases of this table, we observe that in the absence of geometric control ("="), the ECF is about 50 times larger than when we do have geometric control ("L"); the first component (cost of the

control, g) is 20 times bigger and the cost of the final state is twice as big.

- We must have at least one control boundary perpendicular to the direction of the oscillating part of the initial data in order to obtain good convergence – this is the geometric condition.
- Even in the bad case (control on N and S only) we have the same behavior of the L^1 norm of g as a function of T – this phenomenon is thus independent of the control geometry.
- The comparison of $\|g(t)\|_{L^2(\Gamma)}$ for the 2 geometries is interesting (see Figures 10 and 11); the norm of g has an apparently chaotic form for the bad case, whereas when we have one control boundary perpendicular, there is a coherent envelope – this indicates a dependence of the form of $\|g(t)\|_{L^2(\Gamma)}$ on the control geometry.
- The results for the N-S control boundary are not as well converged as the others – in fact we have used a convergence criterion of 10^{-4} here.
- In [1] and [9] explicit observability inequalities with an exponential factor of the form e^{n^α} were obtained for the boundary controllability of a linear hybrid system on the unit square, where n is the frequency of the oscillations in the x-direction.

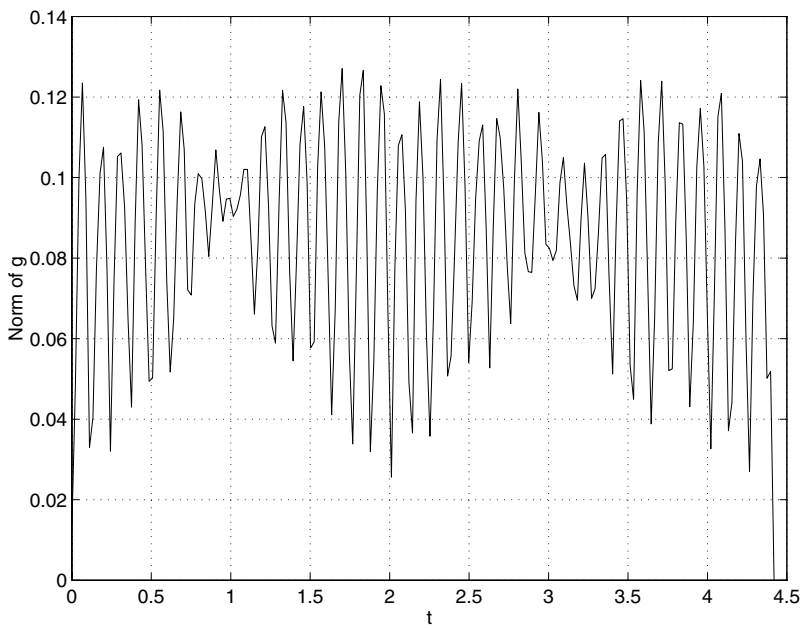

FIGURE 10. $\|g(t)\|$ for "L" control geometry with the oscillatory initial condition.

7. The wave equation on other domains: numerical study

7.1. The square cavity

The square cavity presents two obvious control boundaries: the internal boundary, Γ_2 (hole) and the external boundary, Γ_1 – see Figure 12. We

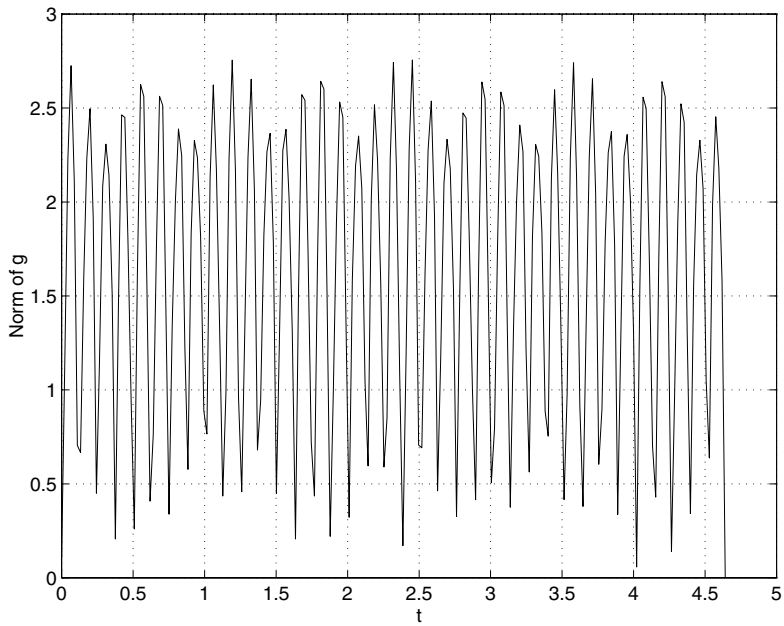

FIGURE 11. $\|g(t)\|$ for "=" control geometry with the oscillatory initial condition.

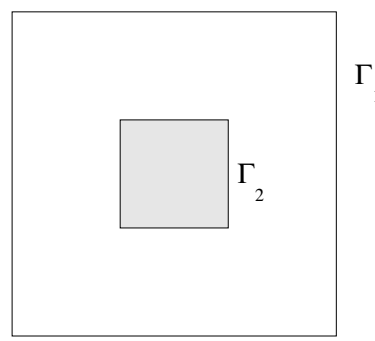

FIGURE 12. The square cavity.

compare these in Table 3. Note that with control on the outer boundary we have geometric controllability, whereas when we control on the hole, there is no geometric controllability.

The three series of animations in Figures 13, 14 and 15 compare the solution of the wave equation *without* any control (Fig. 13) with that obtained when a control is applied

- on the exterior boundary Γ_1 (Fig. 14) and
- on the interior boundary Γ_2 (Fig. 15).

The norms for the Γ_1 control boundary are plotted in Figure 16.

REMARK 7.1.

- Controlling on both boundaries is no better than controlling on the exterior boundary only – there is a very slight difference in the ECF's.

G	T	$\|g\|_{2,\Sigma}$	$\|g\|_{1,\Sigma}$	$\frac{\|u^0-u_c^0\|_{2,\Omega}}{\|u^0\|_{2,\Omega}}$	$\frac{\|u(T)\|_{2,\Omega}}{\|u^0\|_{2,\Omega}}$	ECV	
$\Gamma_1 \cup \Gamma_2$	1.77	0.0579	0.0737	0.0383	0.0474	$[0.58, 0.06] \Rightarrow 0.036$	
Γ_1	1.77	0.0741	0.0945	0.0420	0.0426	$[0.74, 0.07] \Rightarrow 0.052$	
	2.65	0.0576	0.0909	0.0432	0.0345	$[0.71, 0.06] \Rightarrow 0.043$	(a)
	3.98	0.0466	0.0906	0.0431	0.0282	$[0.71, 0.05] \Rightarrow 0.036$	
	5.30	0.0403	0.0908	0.0423	0.0332	$[0.71, 0.05] \Rightarrow 0.037$	
	6.63	0.0362	0.0914	0.0419	0.0307	$[0.71, 0.05] \Rightarrow 0.037$	
Γ_2	5.30	0.2355	0.5268	0.0784	0.0670	$[4.12, 0.11] \Rightarrow 0.439$	

TABLE 3. Exponential data on the square cavity with 2 control geometries; convergence criterion, $\varepsilon = 10^{-5}$; $\alpha = (96, 96)$, $\beta = (0, 0)$; $(x_0, y_0) = (0.8, 0.8)$, $N = 32$; Γ_1 = external boundary, Γ_2 = internal boundary. Notes: $^{(a)}$ $\theta = 0$ fixed and T varying.

- Controlling on the interior boundary requires substantially more time and a much larger control energy – the ECF is approximately 10 times larger (cost of control is 5 times larger, cost of final state is twice as large).
- We once again find the expected dependence of the norms on T, so this dependence appears to be independent of the domain geometry and of the control geometry.

7.2. THE SQUARE WITH TWO CAVITIES

This example is inspired from the "bowling ball" case. We now have three possible control boundaries: the two holes (Γ_2 and Γ_3) and the exterior boundary (Γ_1). The fine discretization mesh is shown in Figure 17. In addition to varying the geometry of the control boundary, we will also examine the effect of the direction of propagation of the initial data. Results are presented in Table 4.

G	T	θ	$\|g\|_{2,\Sigma}$	$\|g\|_{1,\Sigma}$	$\frac{\|u^0-u_c^0\|_{2,\Omega}}{\|u^0\|_{2,\Omega}}$	$\frac{\|u(T)\|_{2,\Omega}}{\|u^0\|_{2,\Omega}}$	ECV	
$\Gamma_1 \cup \Gamma_2$	1.33	0	0.0199	0.0218	0.0550	0.0497	$[0.39, 0.08] \Rightarrow 0.032$	
$\cup \Gamma_3$	1.33	$\pi/2$	0.0200	0.0219	0.0542	0.0500	$[0.40, 0.08] \Rightarrow 0.032$	
Γ_1	2.21	0	0.0357	0.0502	0.0640	0.0890	$[0.91, 0.15] \Rightarrow 0.136$	
	2.21	$\pi/4$	0.0354	0.0497	0.0634	0.0879	$[0.90, 0.15] \Rightarrow 0.132$	(a)
	2.21	$\pi/2$	0.0351	0.0493	0.0629	0.0868	$[0.91, 0.15] \Rightarrow 0.130$	
$\Gamma_2 \cup \Gamma_3$	2.21	0	0.0448	0.0641	0.0863	0.0867	$[1.16, 0.14] \Rightarrow 0.167$	
	2.21	$\pi/4$	0.0452	0.0648	0.0865	0.0875	$[1.17, 0.15] \Rightarrow 0.171$	
	2.21	$\pi/2$	0.0457	0.0654	0.0867	0.0884	$[1.18, 0.15] \Rightarrow 0.175$	
Γ_3	7.73	0	0.0659	0.1799	0.1188	0.1232	$[3.25, 0.22] \Rightarrow 0.717$	(b)

TABLE 4. Exponential data on the 2-cavity square with various control geometries; $(x_0, y_0) = (0.5, 0.5)$, $\alpha = (512, 512)$, $\beta = (2, 0)$; $N = 64$; Γ_1 =external boundary, Γ_2, Γ_3 = internal boundaries. Notes: $^{(a)}$ the minimal control time $T = 1.77$; $^{(b)}$ not converged after 10 iterations; criterion $\varepsilon_c = 4 \cdot 10^{-3}$.

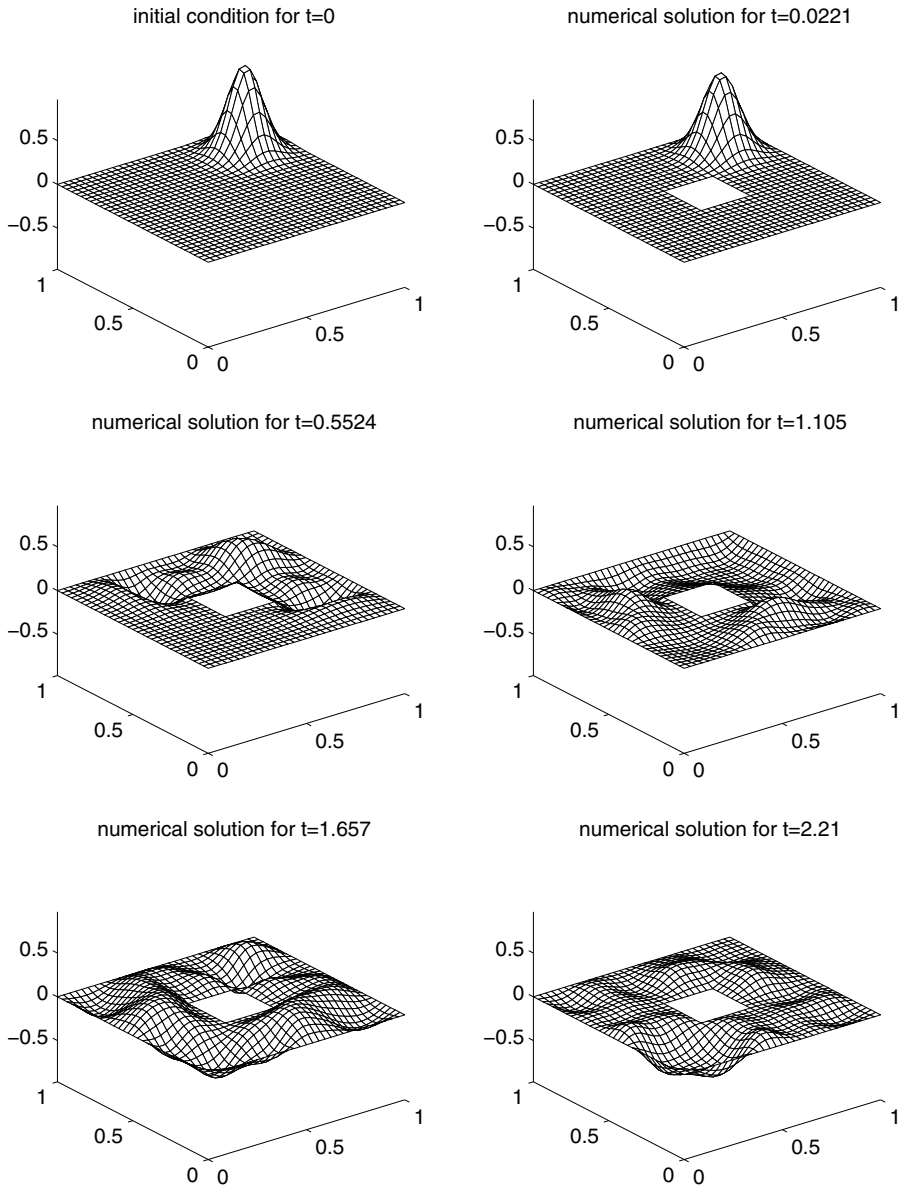

FIGURE 13. Solution of wave equation on square cavity – no control.

REMARK 7.2.

- Controlling everywhere requires the smallest T and gives a small value of the ECF.
- Controlling only on the outer boundary is comparable in cost to controlling on the 2 inner boundaries only.
- The dependence on the angle θ is interesting: when controlling on the outer boundary, the ECF decreases as θ varies from 0 to $\pi/2$ whereas when controlling on the 2 cavities the ECF increases – this shows the effect of controlling in the direction perpendicular to the propagation of the initial data.

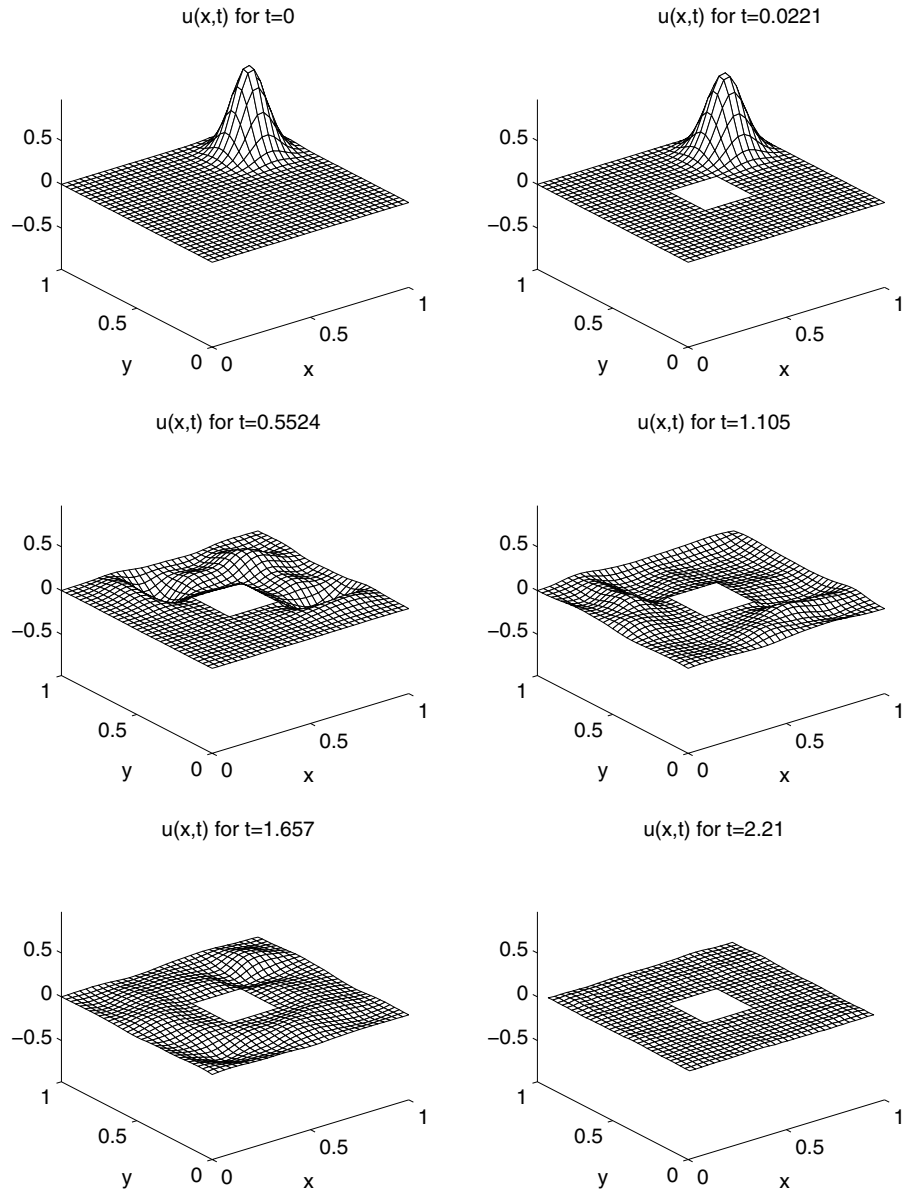

FIGURE 14. Solution of wave equation on square cavity – control on Γ_1.

- Controlling on only one cavity is expensive and convergence is difficult to achieve – the cost of the control, g, is about 10 times larger and the final state is 4 times as big when compared with the case of control on the whole boundary.

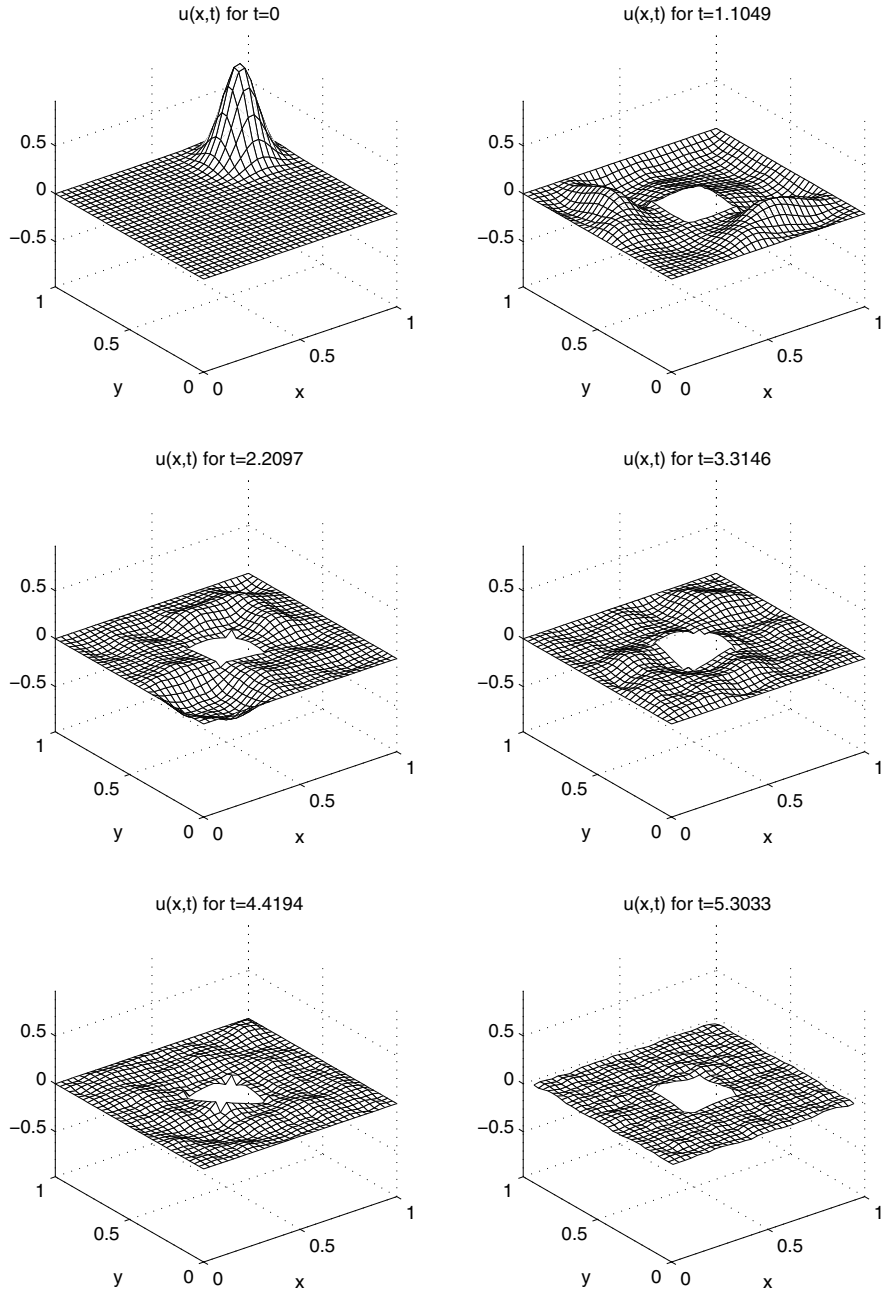

FIGURE 15. Solution of wave equation on square cavity – control on Γ_2.

7.3. The ellipse

Since the boundary of the domain Ω is no longer straight, we need to modify the finite difference scheme. Details of the modifications can be found in Appendix B.

On the ellipse we will first study the case of a nice exponential initial condition and then we will consider oscillatory initial data on two control geometries:

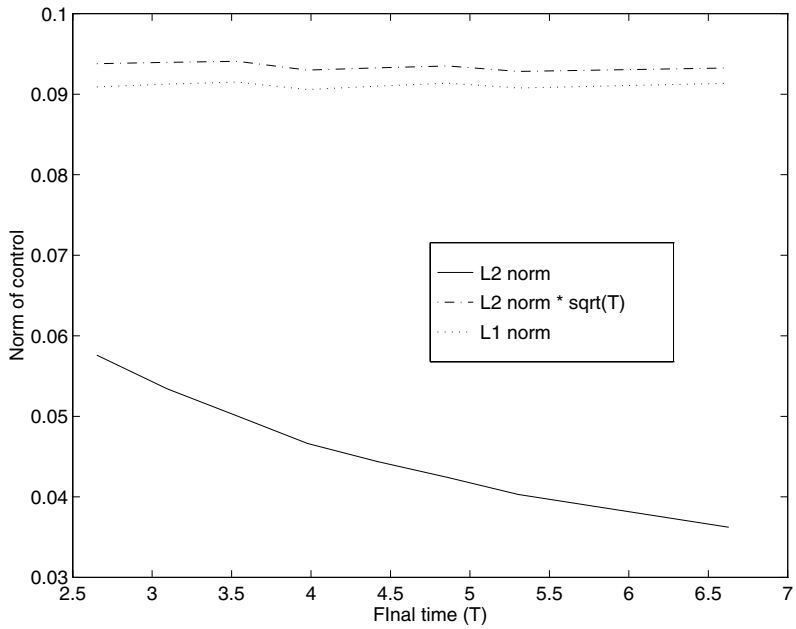

FIGURE 16. $L^1(0,T;L^2(\Gamma))$ and $L^2(\Sigma)$ norms of the boundary control as functions of the control time T for exponential initial condition on the square cavity with control on the outer boundary (Γ_1).

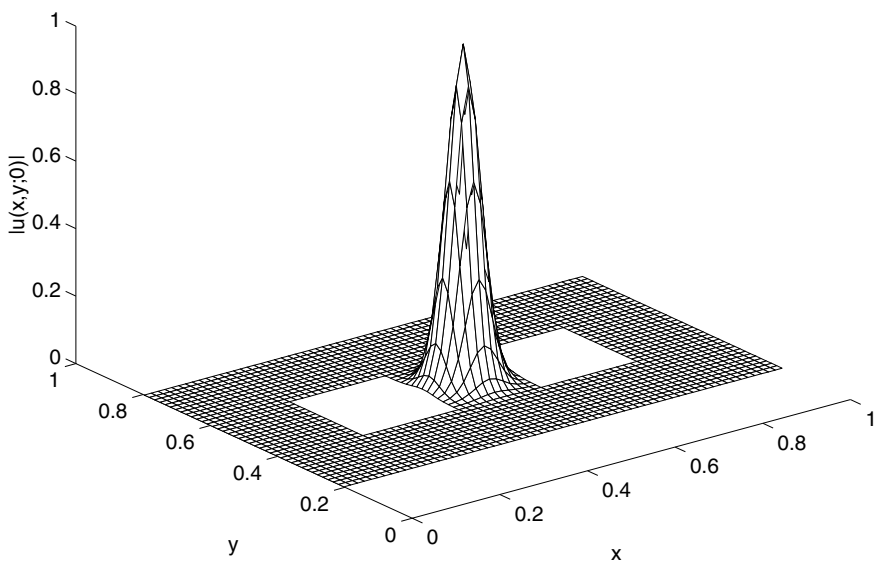

FIGURE 17. Exponential initial condition on fine mesh for the 2-cavity case – N=64.

1. $g = 0$ on the extremities of the minor axis (y) – denoted by $\updownarrow$ – with the data rapidly oscillating in the y direction (see Figure 18);
2. $g = 0$ on the extremities of the major axis (x) – denoted by $\leftrightarrow$ – with the data rapidly oscillating in the x direction.

Results are presented in Tables 5 and 6.

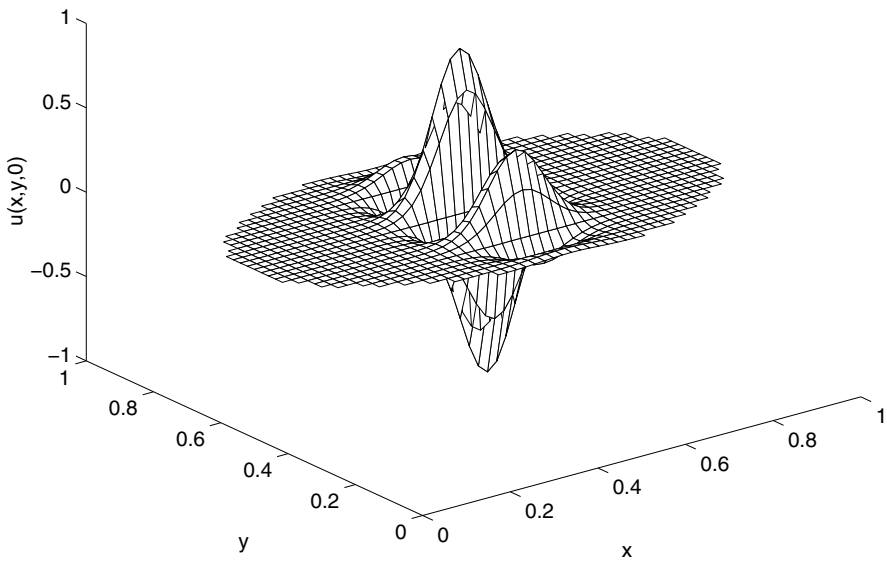

FIGURE 18. Oscillatory initial condition for the ellipse – N=48.

T	$\|g\|_{2,\Sigma}$	$\|g\|_{1,\Sigma}$	$\frac{\|u^0-u_c^0\|_{2,\Omega}}{\|u^0\|_{2,\Omega}}$	$\frac{\|u(T)\|_{2,\Omega}}{\|u^0\|_{2,\Omega}}$	ECV	
1.75	0.0714	0.0896	0.0199	0.0528	$[0.57, 2.54] \Rightarrow 1.455$	(a)
1.8	0.0683	0.0866	0.0174	0.0474	$[0.55, 0.61] \Rightarrow 1.005$	
1.9	0.0660	0.0850	0.0056	0.0091	$[0.54, 0.49] \Rightarrow 0.268$	
2.0	0.0658	0.0859	0.0086	0.0170	$[0.55, 0.61] \Rightarrow 0.332$	
2.25	0.0616	0.0856	0.0140	0.0456	$[0.55, 0.58] \Rightarrow 0.319$	
2.5	0.0591	0.0862	0.0047	0.0077	$[0.55, 0.24] \Rightarrow 0.133$	(b)
2.75	0.0583	0.0882	0.0087	0.0209	$[0.56, 0.56] \Rightarrow 0.316$	
3.0	0.0540	0.0863	0.0074	0.0165	$[0.55, 0.70] \Rightarrow 0.385$	
3.25	0.0513	0.0853	0.0073	0.0167	$[0.54, 0.85] \Rightarrow 0.464$	

TABLE 5. Exponential data on the ellipse with control on entire boundary; $N = 48$, $\alpha = (64, 64)$, $\beta = (0, 0)$. Notes: $^{(a)}$ this value of T is too small for control; $^{(b)}$ for this T, the ECF is minimal.

G	T	$\|g\|_{2,\Sigma}$	$\|g\|_{1,\Sigma}$	$\frac{\|u^0-u_c^0\|_{2,\Omega}}{\|u^0\|_{2,\Omega}}$	$\frac{\|u(T)\|_{2,\Omega}}{\|u^0\|_{2,\Omega}}$	ECV	
$\leftrightarrow$	1.75	0.1125	0.1365	0.0874	0.0667	$[1.15, 13.4] \Rightarrow 15.42$	
	2	0.0981	0.1212	0.0823	0.0679	$[1.02, 8.38] \Rightarrow 8.531$	
	3	0.0830	0.1240	0.1132	0.0712	$[1.04, 17.5] \Rightarrow 18.19$	(a)
	4	0.0715	0.1237	0.1262	0.0730	$[1.04, 20.6] \Rightarrow 21.45$	
	5	0.0586	0.1160	0.1377	0.0694	$[0.97, 19.4] \Rightarrow 18.89$	
$\updownarrow$	2	0.1876	0.1945	0.1247	0.0873	$[1.94, 175] \Rightarrow 340$	
	3	0.1315	0.1717	0.1656	0.1162	$[1.72, 85.6] \Rightarrow 147.1$	(b)
	4	0.1175	0.1765	0.1825	0.0860	$[1.76, 63.3] \Rightarrow 111.6$	
	5	0.09835	0.1680	0.1791	0.0888	$[1.68, 46.8] \Rightarrow 78.59$	
	6	0.0889	0.1667	0.1901	0.0996	$[1.67, 63.8] \Rightarrow 106.4$	

TABLE 6. Oscillatory data on the ellipse with 2 control geometries; $N = 48$. Notes: $^{(a)}$ $\alpha = (24, 128)$, $\beta = (12, 0)$, $\theta = 0$; $^{(b)}$ $\alpha = (48, 128)$, $\beta = (12, 0)$, $\theta = \pi/2$.

REMARK 7.3.

- It is much more difficult to control the oscillatory data – as expected – the ECF's for the exponential data are 2 to 3 orders of magnitude smaller than those of the oscillatory cases.
- If we look at the first components of the ECV (cost of control) we see that the oscillatory cases give values 2 to 4 times larger than the exponential cases; the second components (cost of final state) are 40 to 100 times larger due mainly to the high values of $\|u^1(T)\|_{-1,\Omega}$.
- For the exponential data, we again obtain the previously remarked behavior of the norms of g – the L^1-norm is basically constant with T, whereas the L^2-norm is decreasing.
- The "$\leftrightarrow$" case has ECF's one order of magnitude smaller (factor of 2 in g, factor of 5 in $u(T)$) than those of the "$\updownarrow$" case – the explanation comes from geometrical optics: the trajectory of a wave propagating along the major axis is less stable than that of a wave in the minor axis direction; thus the wave of the minor axis tends to remain in the vicinity of this axis after reflections, and hence stays in the zero control region; on the other hand, due to the instability of the major axis wave, this wave sees the non-zero control boundary more often and is thus more easily controlled.
- The "$\leftrightarrow$" case is optimally controlled (minimal ECF) for small values of T (around $T = 2$) whereas the "$\updownarrow$" case needs much more time and has a minimal ECF around $T = 5$.
- The graphs of $\|g(t)\|_{L^2}$ for the 2 oscillatory cases are interesting to compare (see Figures 19 and 20):
  - the peak amplitudes of the "$\leftrightarrow$" case are half as large as those of the "$\updownarrow$" case since this case is more difficult to control;
  - the periods of the peaks reflect quite precisely the control geometry as well as the geometry of the ellipse: for the "$\leftrightarrow$" case the period is about 1 which corresponds to the length of the major axis; for the "$\updownarrow$" case the period is about 0.6 which is the length of the minor axis.

- We cannot directly compare the ECF's of the ellipse with the previous cases (square geometries) due to the change in numerical method (see Appendix B); however in a forthcoming paper [2] we will use overlapping grids which will treat all geometries with the same precision; when comparing Tables 1 and 5 we note that the g-cost is about the same, but the $u(T)$-cost is 10 times larger.

8. Summary of numerical results

In this section we present two Tables, 7 and 8, which will effectively summarize the numerical results of the previous sections.

G	T	$\|g\|_{1,\Sigma}$	$\frac{\|u(T)\|_{2,\Omega}}{\|u^0\|_{2,\Omega}}$	ECV
$\Gamma_1 \cup \Gamma_2 \cup \Gamma_3$	1.33	0.0218	0.0497	$[0.39, 0.08] \to 0.032$
Γ_1	2.21	0.0502	0.0890	$[0.91, 0.15] \to 0.136$
$\Gamma_2 \cup \Gamma_3$	2.21	0.0641	0.0867	$[1.16, 0.14] \to 0.167$
Γ_3	7.73	0.1799	0.1232	$[3.25, 0.22] \to 0.717$

Table 7. Exponential data on the 2-cavity square with various control geometries; $(x_0, y_0) = (0.5, 0.5)$, $\alpha = (512, 512)$, $\beta = (2, 0)$; $N = 64$; Γ_1 =external boundary, Γ_2, Γ_3 = internal boundaries.

Table 7 summarizes the results obtained in the two-cavity case. Here we clearly observe the following:

1. as the size of the control boundary decreases, the time needed to control increases;
2. as the control boundary becomes smaller, there are more and more trapped rays and the control energy in the ECV (first term) increases first by a factor of 3 as we move from the entire boundary to the internal boundaries only, and then by a further factor of 3 as we control on one cavity only;
3. the overall ECF (product of the two components) increases correspondingly and thus indicates well the loss of geometric controllability.

G	T	$\|g\|_{1,\Sigma}$	$\frac{\|u(T)\|_{2,\Omega}}{\|u^0\|_{2,\Omega}}$	ECV
$\longleftrightarrow$	2	0.1212	0.0679	$[1.02, 8.38] \to 8.531$
	4	0.1237	0.0309	$[1.04, 20.6] \to 21.45$
$\updownarrow$	2	0.1945	0.0873	$[1.94, 175] \to 340$
	4	0.1765	0.0860	$[1.76, 63.3] \to 111.6$

Table 8. Oscillatory data on the ellipse with 2 control geometries; $N = 48$.

In Table 8 we present the principal results for the ellipse. We observe that:

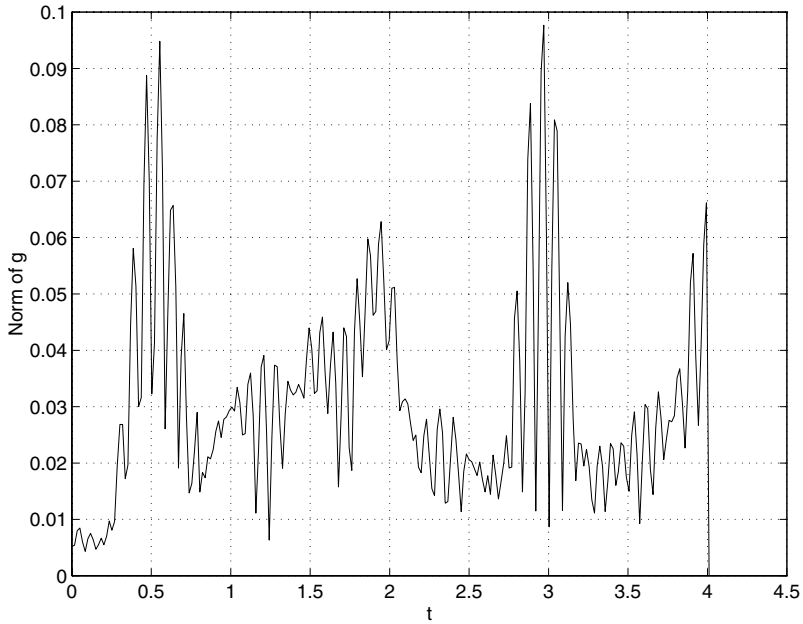

FIGURE 19. $\|g(t)\|$ for oscillatory data on the ellipse with zero control on the *major* axis.

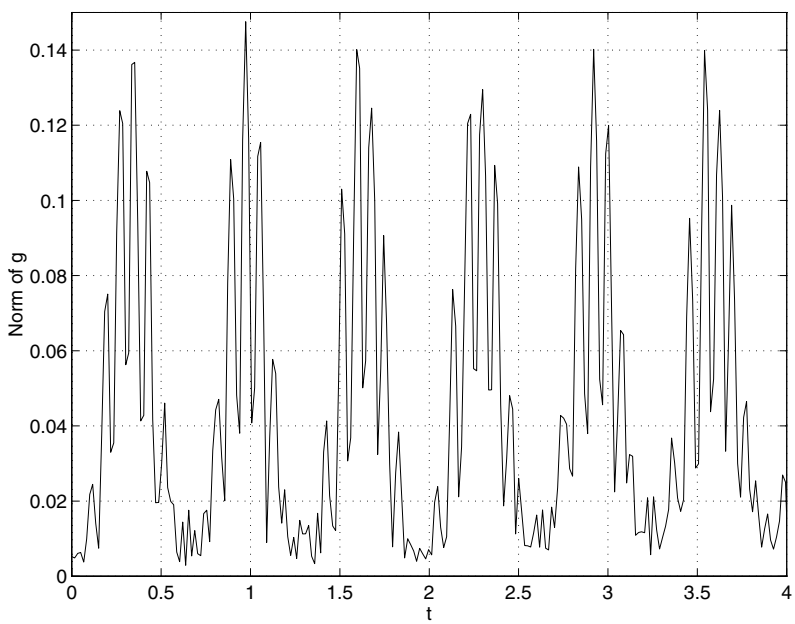

FIGURE 20. $\|g(t)\|$ for oscillatory data on the ellipse with zero control on the *minor* axis.

1. for the stable ray which propagates along the minor axis, we need a larger energy to control than for the unstable ray along the major axis;
2. the ECF is very large in the case where we do not have geometric controllability.

9. Conclusions

This extensive numerical study of the geometrical aspects of boundary controllability has provided us with an improved understanding of the nature of the control function g. We have observed the following:

1. an $L^1(0,T\,;\,L^2(\Gamma_0)\,)$ norm of g provides a better estimate of the *total* amount of energy needed to control a given configuration;
2. the ECF enables us to compare *quantitatively* the cost of control for different control geometries and for different initial conditions;
3. the magnitude of the ECF is related to the geometric controllability: when the ECF is large, there are trapped rays and we are thus in a case where there is a loss of geometric controllability;
4. the form of the time dependence of $\|g(t)\|_{L^2(\Gamma)}$ is related to the geometry and to the controllable or oscillatory nature of the initial data.

We have also been able to corroborate results stemming from geometrical optics. Namely,

1. that with certain control geometries it is far more difficult to achieve the exact controllability because of rays that are trapped – see the two-cavity square example;
2. and that on an ellipse, a ray propagating along the direction of the major axis is less stable than one propagating along the minor axis, whose stability is due to a "focussing" effect.

These results are hopefully applicable to the determination of *radar signatures* for complicated, non-convex geometries where the phenomenon of trapped rays is a significant factor. Indeed, we plan to implement a fully three dimensional version of the code on a supercomputer in order to study this type of problem.

Appendix A. Control on a part of the boundary: theoretical aspects

We now analyze more precisely what happens in the case of control on a *part* of the boundary.

We rewrite our *forward* wave equation in the form:

$$\begin{aligned} (\partial_t^2 - \Delta)\phi &= 0, && \text{(A.1)}\\ \underline{\phi} = \{\phi^0, \phi^1\} &\in E = H_0^1(\Omega) \times L^2(\Omega), \\ \phi\,|_\Gamma &= 0\,. && \text{(A.2)} \end{aligned}$$

If we define

$$K(\phi) = \partial_n \phi|_{\Gamma_0 \times (0,T)},$$

then the operator

$$K : E \to L^2\left(\Gamma_0 \times (0,T)\right)$$

is continuous since a direct inequality gives

$$\|\partial_n \phi\|_{L^2(\Gamma_0 \times (0,T))} \leq c \|\underline{\phi}\|_E \ .$$

The semi-norm induced by K on E will be denoted by $|||\cdot|||$. If T is sufficiently large, K is injective and $|||\cdot|||$ is a norm on E.

Now, the *backward* wave equation is given by

$$\begin{aligned} &(\partial_t^2 - \Delta)\psi = 0, \\ &\psi|_{t=T} = \partial_t \psi|_{t=T} = 0, \\ &\psi|_{\Gamma_0 \times (0,T)} = g, \ \ \psi|_{\Gamma \setminus \Gamma_0 \times (0,T)} = 0, \end{aligned} \tag{A.3}$$

with $g \in L^2(\Gamma_0 \times (0,T))$. We define now an operator $S : L^2(\Gamma_0 \times (0,T)) \to E'$ as

$$S(g) = \{\psi|_{t=0}, \partial_t \psi|_{t=0}\} \in E'.$$

We can easily obtain a relationship between the operators K and S by taking the inner product and integrating by parts:

$$\begin{aligned} 0 &= \int_Q (\partial_t^2 - \Delta)\phi \ \psi \ dx \ dt \\ &= [(\phi_t \, \psi) - (\phi \, \psi_t)]_0^T + \int_0^T \int_{\Gamma_0} (\partial_n \phi) \ \psi \ d\Gamma \ dt. \end{aligned}$$

Hence

$$\begin{aligned} \int_0^T \int_{\Gamma_0} (\partial_n \phi) \ g \ d\Gamma \ dt &= < \phi^1, \psi^0 > - < \phi^0, \psi^1 > \\ &\doteq < \underline{\phi}, S(g) > \end{aligned}$$

and we obtain finally our key expression

$$\int_0^T \int_{\Gamma_0} K(\phi) g \, d\Gamma \, dt = < \underline{\phi}, S(g) > . \tag{A.4}$$

This expression has a number of consequences. Firstly, we make the following definition:

DEFINITION A.1. The space of controllable data is the image of S, $\operatorname{Im} S$, a Hilbert space,

$$\operatorname{Im} S = L^2(\Gamma_0 \times (0,T)) / \ker S.$$

Secondly, we have the following relation:

$$\operatorname{Im} S \text{ dense } \Leftrightarrow K \text{ injective},$$

which follows directly from our key expression (A.4) and is true as long as $T > 2 \max\{\operatorname{dist}(x, \Gamma_0), x \in \Omega)\}$ by the Holmgren uniqueness theorem ("dist" is the geodesical distance). Finally, we have the proposition that the following statements are equivalent:

1. exact controllability;
2. $\operatorname{Im} S = E'$;
3. there exists a constant, c, such that

$$\|\underline{\phi}\|_E \leq c \|K \underline{\phi}\|_{L^2(\Gamma_0 \times (0,T))} \cdot \tag{A.5}$$

The equivalence between the first two statements is the definition of exact controllability. We prove the equivalence between the last two. The proof uses the Riesz lemma: there exists an $h \in E'$ with $\|h\|_{E'} = \|\underline{\phi}\|_E$ such that

$$\|\underline{\phi}\|_E^2 = < \underline{\phi}, h > .$$

Now, if $\operatorname{Im} S = E'$ then $h = S(g)$ with

$$\|g\|_{L^2(\Sigma_0)} \leq c\|\underline{\phi}\|_E.$$

But,

$$\begin{aligned} \|\underline{\phi}\|_E^2 &= < \underline{\phi}, S(g) > \\ &= \int_{\Sigma_0} K(\phi) g \; d\Gamma \, dt \\ &\leq \|K(\phi)\|_{L^2(\Sigma_0)} \|g\|_{L^2(\Sigma_0)}, \end{aligned}$$

and thus

$$\|\underline{\phi}\|_E \leq c\|K\underline{\phi}\|_{L^2(\Sigma_0)}.$$

On the other hand, if

$$\|\underline{\phi}\|_E \leq c\|K\underline{\phi}\|_{L^2(\Sigma_0)}$$

then $\operatorname{Im} K$ is closed in $L^2(\Sigma_0)$. Thus

$$L^2(\Sigma_0) = \operatorname{Im} K \oplus (\operatorname{Im} K)^{\perp} \tag{A.6}$$

and we can identify $E = \operatorname{Im} K$. Finally, if $h \in E'$, then $< \underline{\phi}, h >$ is a linear, continuous form on E and thus of the form

$$< \underline{\phi}, h >= \int_{\Sigma_0} K(\phi) g \; d\Gamma \, dt \, .$$

But

$$\int_{\Sigma_0} K(\phi) g \; d\Gamma \, dt = < \underline{\phi}, S(g) >,$$

thus

$$h = S(g).$$

Once we have the estimate (A.5) which is equivalent to $\operatorname{Im} S = E'$, we can formulate the problem of optimal control: "given an h with $< \underline{\phi}, h >$ a linear form on E, what is the g with *minimal* norm such that

$$< \underline{\phi}, h >= \int_0^T \int_{\Gamma_0} K(\phi) g \; d\Gamma \, dt?"$$

Using the decomposition (A.6), we define g_0 as the projection of g onto $\operatorname{Im} K$. This is the control of minimal norm, and

$$g_0 = K(w_0) = \partial_n w_0|_{\Gamma_0 \times (0,T)} \, .$$

So

$$\int_0^T \int_{\Gamma_0} \partial_n \phi \; \partial_n w_0 \; d\Gamma \, dt = < \underline{\phi}, S(g_0) >$$

and if $\phi = w_0$ then

$$< \underline{\phi}, S(g_0) >= \langle \Lambda(w_0), w_0 \rangle \, .$$

When the estimate (A.5) holds and if T is large enough to ensure that K is injective, then $\langle \Lambda(e), e' \rangle$ is a scalar product equivalent to $(\cdot, \cdot)_E$.

Finally, in the general case, we attribute to E the norm

$$\|K(\phi)\| \doteq |||\underline{\phi}|||$$

and we *complete* E in this norm in order to obtain the space F. As a result, Λ defines an isomorphism from F onto $F' = \operatorname{Im} S$, a dense subset of E'.

REMARK A.2. The operator Λ constructs the control of *minimal* norm in $L^2(\Gamma_0 \times (0,T))$.

REMARK A.3. When T is large enough, $\operatorname{Im} S$ is dense, and we can always (in theory) find a control g_ε such that the final state is of norm ε. However, if we do *not* have exact controllability (due to geometrical considerations in particular), then $\|g_\varepsilon\|$ can tend to infinity as $\varepsilon \to 0$. This crucial point justifies the introduction of a new criterion for the appraisal of solutions (see Section 5.2) which takes into account both

- the closeness (ε) of the final state to zero, *and*
- the norm of the control ($\|g_\varepsilon\|$) or energy expended in order to attain this final state.

APPENDIX B. FINITE DIFFERENCES ON A CURVED BOUNDARY

In this appendix we explain the improvement techniques used for the finite difference scheme in the vicinity of a curved boundary. For an accurate method, we require that the governing difference equation applies at *every* internal point. The points neighboring the boundary (internal to or on) will be called *boundary points*. There are two types: *irregular* boundary points (point A in the figure) which do not have all 4 neighbors inside the region, and *regular* boundary points whose neighbors are all inside or on the boundary. The approach most frequently recommended in the literature is that at an irregular boundary point we must *modify* the regular computational molecule (the 5-point discrete Laplacian) by taking into account the irregular spacings (λ_1 and λ_3) and the boundary conditions. This method is quite complex and gives very disappointing results when the solution becomes oscillatory. It is thus *not* at all suitable for the solution of the wave equation whose very nature is to propagate oscillatory solutions indefinitely, without any damping. This fact was remarked by [10].

B.1. THE 9-POINT FINITE DIFFERENCE SCHEME FOR THE WAVE EQUATION

Following the advice of [10], we still use an explicit finite difference approximation scheme for the wave equation but we approximate the Laplacian operator by an $O(h^6)$ scheme based on 9 points with a stencil

$$\Delta_h = \begin{bmatrix} 1 & 4 & 1 \\ 4 & -20 & 4 \\ 1 & 4 & 1 \end{bmatrix}$$

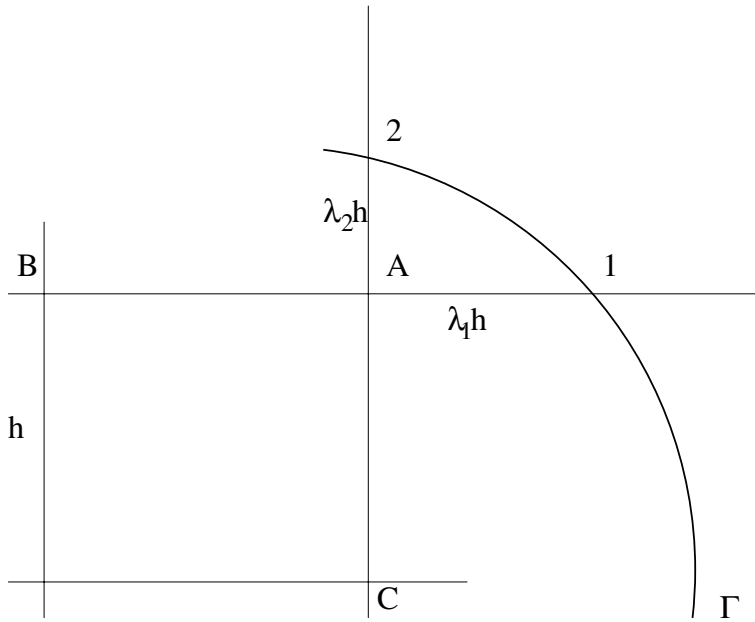

FIGURE 21. Geometry of an irregular boundary point A.

and thus

$$\begin{aligned} 6h^2\Delta u = 4\left[u_{i-1,j} + u_{i+1,j} + u_{i,j-1} + u_{i,j+1}\right] \\ + u_{i-1,j-1} + u_{i+1,j-1} + u_{i-1,j+1} + u_{i+1,j+1} \\ - 20u_{ij} + O(h^6)\,. \end{aligned}$$

This yields the following discretization of the wave equation at an interior point with coordinates (ih, jh):

$$\begin{aligned} u_{ij}^{n+1} = \frac{2}{3}r^2\left(u_{i-1,j}^n + u_{i+1,j}^n + u_{i,j-1}^n + u_{i,j+1}^n\right) \\ + \frac{r^2}{6}\left(u_{i-1,j-1}^n + u_{i+1,j-1}^n + u_{i-1,j+1}^n + u_{i+1,j+1}^n\right) \\ + 2\left(1 - \frac{5}{3}r^2\right)u_{ij}^n - u_{ij}^{n-1}, \end{aligned}$$

where $r = (\Delta t)/h$ and $t = n(\Delta t)$. The stability condition for this scheme is given by

$$\Delta t \leq \sqrt{\frac{13 - \sqrt{61}}{8}}h \approx 0.8054h.$$

B.2. IMPLEMENTATION

In order to implement the 9-point scheme, we extend the mesh to include all necessary points in the neighborhood of the irregular boundary points. When the boundary condition is non-zero as in the case of the ψ wave equation, we assign the boundary values to the mesh points *exterior* to or *on* the boundary. Recall that these values are actually the normal derivatives of ϕ at the boundary. These normal derivatives are calculated on the points just inside the boundary (the irregular boundary points) and then assigned

to the corresponding exterior points. If an exterior point has no interior neighbor, it is assigned a zero boundary value.

This artifice of extending the mesh does not produce the spurious spikes which we observe when using a modified scheme which takes into account the irregular mesh spacings, or when using the usual 5-point scheme.

Appendix C. Convergence of the conjugate gradient algorithm

In this appendix we present some convergence results for our algorithm.

C.1. Convergence and mesh size

This first example will study the convergence of the conjugate gradient algorithm as a function of the mesh size, h. We take a unit square with smooth exponential initial data and a fixed control time, $T = 3$. We stop the iterations at the point where the calculated convergence criterion, ε_c, starts to increase. If one would like to think in terms of a constant convergence criterion, we could say that all results converged to $\varepsilon = 5 \cdot 10^{-6}$. The results are presented in Table 9.

h	T	#	ε_c	$\frac{\|u^0 - u_c^0\|_{2,\Omega}}{\|u^0\|_{2,\Omega}}$	$\frac{\|u(T)\|_{2,\Omega}}{\|u^0\|_{2,\Omega}}$	ECF
1/16	3	4	$1.7 \cdot 10^{-6}$	0.0914	0.0620	0.0630
1/32	3	4	$2.1 \cdot 10^{-6}$	0.0186	0.0206	0.0207
1/64	3	4	$1.1 \cdot 10^{-6}$	0.0096	0.0132	0.0115

Table 9. Exponential data on the unit square with control on entire boundary; $\alpha = (64, 64)$, $\beta = (0, 0)$; $T = 3$.

Remark C.1. We can observe the following:

- the number of iterations required to attain ϵ_c is independent of the mesh size;
- as h decreases, the precision of the results increases – from a 10% error for $h = 1/16$ down to an error of about 1% for $h = 1/64$;

C.2. Convergence and control time

In order to study the relationship between the convergence and the time of control, T, we will take the square cavity geometry with control on the exterior boundary. As before (see Section 7.1) we use exponential initial data localized in the upper right corner. The convergence tolerance is taken as $\varepsilon = 1 \cdot 10^{-5}$. In Figure 22 we plot the number of iterations required to converge versus the control time. We observe that for small values of T, we need a large number of conjugate gradient iterations, whereas from $T \approx 2$ the number of iterations stabilizes at 4. The explanation of this is easily made. Look again at Figure 13. We observe that around $t = 1.6$ the initial data has made a complete circuit of the cavity. Thus the effective diameter of the geometry must be around this value (assuming a unit velocity) and for smaller values of T, the control will be difficult to achieve. Once the minimal time to control is passed, the control is equally easy for all $T > T_{\min}$.

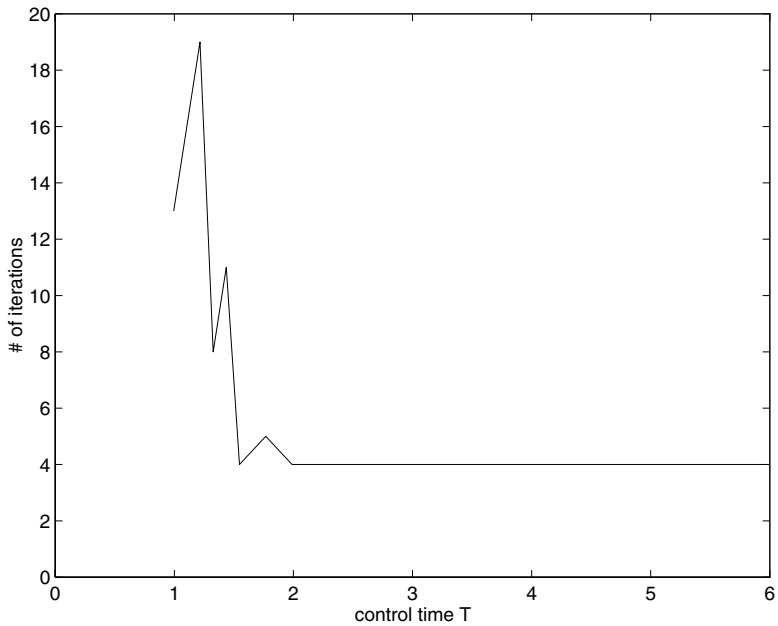

FIGURE 22. Number of conjugate gradient iterations versus the control time, T, for the square cavity.

C.3. CONVERGENCE AND OSCILLATORY INITIAL DATA

Here we will compare the convergence results of controllable and oscillatory initial conditions. We take a curved geometry: the ellipse of Section 7.3. In Table 10 we present these 2 cases. We observe the following:

1. with the controllable data, we can converge to $\varepsilon_c < 10^{-5}$ as was the case for the square geometries;
2. when the data is oscillatory, we can only attain a tolerance of 10^{-4} – this was also observed on the square geometries;
3. the oscillatory cases require more iterations to converge (from 6 to 8) than the controllable cases (from 4 to 5 iterations).

T	#	ε_c	$\frac{\|u^0-u_c^0\|_{2,\Omega}}{\|u^0\|_{2,\Omega}}$	$\frac{\|u(T)\|_{2,\Omega}}{\|u^0\|_{2,\Omega}}$	ECF	Note
3	4	$9.8 \cdot 10^{-6}$	0.0074	0.0165	0.3856	(a)
3	6	$7.8 \cdot 10^{-5}$	0.1132	0.0712	18.19	(b)
3	8	$1.6 \cdot 10^{-5}$	0.1656	0.1162	147.1	(c)

TABLE 10. Controllable and oscillatory data on the ellipse: $N = 48$. Notes: $^{(a)}$ controllable data: $\alpha = (64, 64)$, $\beta = (0, 0)$; $^{(b)}$ oscillatory data: $\alpha = (24, 128)$, $\beta = (12, 0)$, $\theta = 0$, "$\leftrightarrow$" geometry; $^{(c)}$ oscillatory data: $\alpha = (48, 128)$, $\beta = (12, 0)$, $\theta = \pi/2$, "$\updownarrow$" geometry;

Appendix D. Use of MATLAB for solution of the wave equation

In this appendix, we show an example of the usage of the MATLAB program. We solve the wave equation on a general domain using a very efficient matrix-vector formulation. MATLAB is ideal for this kind of algorithm. Here is the program:

```
% Solve the (forward) wave-equation
%      BOX(u) = 0, in Omega x (0,T)
%      u = f(x,y)  on dOmega, t > 0 (== Sigma)
%      u = u0(x,y,0) , du/dt = u1(x,y,0) in Omega
%
% by an explicit finite-difference scheme,
%(central-differences)
clear

% INPUT:

Ih = input('Number of spatial elements in x-
                                    and y-directions = ');
N  = input('# of time steps  = ');

% choose a geometry:
K=menu('GEOMETRY','square','L','L w/ circle','disc',...
       'annulus','cardioid','butterfly');
if K==1 , GG='S';
  elseif K==2, GG='L'; elseif K==3, GG='C';
  elseif K==4, GG='D'; elseif K==5, GG='A';
  elseif K==6, GG='H'; else GG='B';
end

% discretization parameters:
I=Ih+1; h=2/Ih; k=h/sqrt(2); r=(k/h);
x=0:h:1; y=0:h:1;
[X,Y]=meshdom(x,y);

disp(sprintf('Space discretization, h = %g',h))
disp(sprintf('Time discretization, k  = %g',dt))
disp(sprintf('Number of time steps,N  = %g',N))
disp(sprintf('Final time ,T  = %g',N*dt))


% Generate and display the grid

   G = numgrid(GG,Ih+1);
   spy(G); title('A finite difference grid ')
   disp('pause'), disp(' '), pause
```

```
% Generate and display the discrete d'Alembertian.

   D = delsqr(G,r);
   spy(D); title('The 5-point d'Alembertian')
   disp('pause'), disp(' '), pause

% Assume a ZERO boundary condition
   bc=zeros(I,I);

% Set-up initial conditions in interior
   x0 = 0.5; y0 = 0.5;
   u0 = exp( -64( (X-x0).^2 + (Y-y0).^2 ) );
   u1 = zeros(I,I);

% Plot the initial condition:
   mesh(X,Y,u0); axis([0 1 0 1 -.6 .6]);
   title(' Initial condition, u0'); pause;

% SOLVE the wave-equation:

% Convert matrix interior -> vector

   u0 = u0(G>0); u1=u1(G>0);

% First time step:

   unm1=u0;
   un = 0.5*D*u0 + k*u1;

% Map the solution onto the grid and display results
   Un = G;
   Un(G>0) = full(un(G(G>0)));
   mesh(X,Y,Un); axis([-1 1 -1 1 -.6 .6]);
   title([' numerical solution for t=',num2str((+1)*k)])
   pause;

% Loop on time:

disp('Looping on time ...')

for nt=1:Nt

  % Assign boundary condition to un (if non-zero)
  % Solve for t=n+1

     unp1 = D*un - unm1;

  % Update (except for last step)
```

```
    if nt < Nt
      unm1 = un  ;
      un   = unp1;
    end

  % Map the solution onto the grid and display results
    Unp1 = G;
    Unp1(G>0) = full(unp1(G(G>0)));
    mesh(X,Y,Unp1); axis([-1 1 -1 1 -.6 .6]);
    title([' numerical solution for t=',num2str((nt+1)*k)])
    pause;

end % of time loop
```

Some remarks are in order:

1. all routines called are standard, with the exception of `delsqr` which is an obvious modification of the standard routine `delsq` of Matlab to calculate the discrete Laplacian;
2. Matlab calculates and stores the finite difference matrix, `D`, in a sparse form, and consequently *all* computations in the time loop use very efficient sparse algorithms;
3. in order to speed up the execution times even further, one should eliminate all conditionals that are inside the time loop.

This routine is at the heart of our HUM program, and thanks to its obvious efficiency we have been able to perform all our numerical simulations on PC's and Sun workstations.

The authors would like to thank the referees for their thorough work and their constructive propositions which greatly improved the final form of this article.

List of Figures

References

[1] B. Allibert: *Contrôle analytique de l'équation des ondes sur des surfaces de révolution*, PhD thesis, École Polytechnique, 1997.

[2] M. Asch: Control and stabilization of wave propagation problems on complex geometries, *in preparation*, 1998.

[3] M. Asch, B. Vai: Une étude numérique du contrôle exacte du système de l'élasticité linéaire en dimension deux, *Technical report 98-05*, Laboratoire de Mathématiques, Université Paris-Sud, 1998.

[4] C. Bardos, G. Lebeau, J. Rauch: Sharp sufficient conditions for the observation, control and stabilization of waves from the boundary, *SIAM Journal of Control and Optimization*, **30**, 1992, 1024–1065.

[5] I. Charpentier, Y. Maday: Idetifications numériques de contrôles distribués pour l'équation des ondes, *C. R. Acad. Sci. Paris Série I*, **322**, 1996, 779–784.

[6] R. Glowinski: Ensuring well-posedness by analogy; Stokes problem and boundary control for the wave equation, *Journal of Computational Physics*, **103**, 1992, 189–221.
[7] R. Glowinski, C.-H. Li, J.-L. Lions: A numerical approach to the exact controllability of the wave equation (I) Dirichlet controls: description of the numerical methods, *Japan Journal of Applied Mathematics*, **7**, 1990, 1–76.
[8] J.-L. Lions: *Controlabilité exacte, perturbations et stabilisation de systèmes distribués,* Tome I, Collection RMA, Masson, 1988.
[9] S. Micu, E. Zuazua: Boundary controllability of a linear hybrid system arising in the control of noise, *SIAM Journal of Control and Optimization*, **35**, 1997, 1614–1637.
[10] W.E. Milne: *Numerical solution of differential equations*, Dover Publications Inc., 1954.